Deep-Sea Research II 117 (2015) 65–85

Contents lists available at ScienceDirect

Deep-Sea Research II

journal homepage: www.elsevier.com/locate/dsr2

Controls on temporal and spatial variations of phytoplankton pigment distribution in the Northern South China Sea

Tung-Yuan Ho*, Xiaoju Pan, Hsu-Han Yang, George, T.F. Wong, Fuh-Kwo Shiah

Research Center for Environmental Changes, Academia Sinica, Taipei, Taiwan

ARTICLE INFO

Available online 29 May 2015

Keywords:
South China Sea
Pigment
Phytoplankton
Community structure

ABSTRACT

The seasonal and spatial variations of phytoplankton pigment distribution and their interaction with environmental controlling parameters were investigated in the Northern South China Sea (NSCS) at 37 stations covering the coastal region, the continental shelf, the slope, and the deep-water basin during two summer and two winter cruises from 2010 to 2012. Strong spatial, interseasonal, and intraseasonal variations of pigment distribution were observed in the diverse biogeochemical regions, exhibiting extremely dynamic phytoplankton community structure in the NSCS. In addition to chlorophyll *a*, the major pigments observed included divinyl chlorophyll *a* (DV Chl *a*), total chlorophyll *b* (Chl *b*), zeaxanthin (Zea), 19′-hexanoyloxyfucoxanthin (Hex), 19′-but-fucoxanthin (But), fucoxanthin (Fuco), and prasinoxanthin (Pras). Overall, Fuco, Chl *b*, Zea, Hex, But, and Pras were the dominant pigments in the coastal and shelf region; DV Chl *a*, Chl *b*, Hex, But, Zea, and Fuco were the major pigments in the offshore water. After analyzing marker pigment correlations and cellular pigment concentrations, we conclude that Zea, Hex (with But), and Fuco can be used as specific marker pigments for *Synechococcus*, coccolithophores, and diatoms in the NSCS, respectively. We have also derived that prasinophytes accounted for most of the elevated Chl *b* observed in the coastal water and appeared to be an important pico-eukaryotic group (Pico) in the coastal region. With varying cellular pigment concentrations observed vertically and seasonally, it is essential to separate sampling stations to different biogeochemical domains to apply pigment to Chl *a* ratios to estimate phytoplankton community structure in the NSCS. We observed close association between soluble reactive phosphate and Chl *a* abundance in coastal, shelf, and deep-water regions during summer cruises. Major nutrient supply appears to be the main controlling factor on the temporal and spatial variations of major pigment distribution. The supply is mainly driven by terrestrial input in summer and water mixing strength in winter. During the summer periods, major nutrients are primarily supplied from riverine and groundwater discharge; during winter periods, strong winter monsoon intensifies sub-surface water mixing and results in nutrient and pigment elevation in the euphotic zone. Also driven by the monsoon, the intrusion of the low-temperature coastal current from Taiwan Strait to the coastal region of the NSCS may replace or alter the phytoplankton community in the coastal region in winter. Overall, the temporal and spatial variations of phytoplankton pigment distribution in the NSCS are regulated by the fluctuations of these two major environmental forcings.

1. Introduction

Phytoplankton plays a central role for material cycling through the biological pump in the ocean. Understanding phytoplankton abundance and community structure is critical for quantifying and understanding how biologically active material is cycled and transported in the ocean. Both phytoplankton common pigments and phylum specific marker pigments are useful parameters to estimate total phytoplankton biomass and their community structure in the ocean. For example, chlorophyll *a* (Chl *a*) has been widely used to estimate total phytoplankton biomass and primary production in the ocean (Behrenfeld and Falkowski, 1997). The concentrations of some specific marker pigments may be linearly correlated with the biomass of their corresponding phytoplankton groups. For example, divinyl chlorophyll *a* (DV Chl *a*), a unique pigment for *Prochloroccocus* (*Pro*), is used to estimate the abundance and the distribution of *Pro* when the ratio of marker pigment to total Chl *a* is known (Goericke and Repeta, 1993). However, some marker pigments exist in several different phytoplankton groups. For example, Zea exists in *Synechococcus* (*Syn*),

* Corresponding author.
E-mail address: tyho@gate.sinica.edu.tw (T.-Y. Ho).

http://dx.doi.org/10.1016/j.dsr2.2015.05.015
0967-0645/

prasiophytes, and chlorophytes; Chl *b* exists in prasiophytes, chlorophytes, and englenophytes. Numerical computer programs, such as CHEMTAX, have thus been developed to utilize multiple pigment markers and factor analysis to assess the relative contribution of major phytoplankton classes to total Chl *a* concentrations and to quantify relative species percentages in oceanic water (Mackey et al., 1996; Latasa, 2007).

Since different phytoplankton groups possess different marker pigments and ecological niches, both chemical and physical parameters of environmental conditions concurrently influence the distribution of phytoplankton's marker pigment composition in oceanic waters. For example, cyanobacteria, including *Pro* and *Syn*, possess unique ecological niche to survive in oligotrophic waters; dinoflagellates and diatoms are able to dominate in relatively eutrophic water. Understanding the influence of environmental control on the spatial and temporal variations of phytoplankton pigment distribution would provide essential information to utilize pigment composition to quantify community structure and its response to environmental changes. This kind of study may be particularly challenging in marginal seas, where both environmental conditions and phytoplankton community structure vary extensively with time and location. The Northern South China Sea (NSCS), one of the largest marginal seas in the world, is a biogeochemically extremely dynamic oceanic province both temporally and spatially. The biogeochemistry of this tropical sea is driven by diverse anthropogenic and natural forcings at strengths that are among the strongest in the world (Wong et al., 2015). The major forcings include large riverine and submarine groundwater discharges with high nutrient loading (Liu et al., 2012), high atmospheric deposition with material from multiple natural and anthropogenic origins (Ho et al., 2010), different seasonal monsoons with varying directions and strengths, typhoons occurring with high frequencies and strengths, frequently occurring cold and warm eddies, internal waves with the highest amplitudes in the world, and the intrusion of the western boundary current, the Kuroshio water.

Several previous studies have reported the temporal and spatial variations of pigment and phytoplankton community information in the NSCS (e.g., Ning et al., 2005; Cai et al., 2007; Chen et al., 2011; Huang et al., 2010). Most of the published studies focus on investigating the abundance of *Pro*, *Syn*, and Pico by pigment analysis or using flow cytometer in a limited region of the NSCS. Chen et al. (2011) reported seasonal variation patterns for *Pro*, *Syn*, and Pico in the NSCS on one summer and one winter cruises. The study by Zhai et al. (2011) investigated phytoplankton pigment patterns and reported the community composition by using CHEMTAX near the Pearl River in February 2009. Huang et al. (2010) found that different origins and ages of eddies are important processes influencing the variations of phytoplankton community in the NSCS. Using a multiple parameter approach by combining data obtained from satellite images, pigment concentrations, and phytoplankton abundance, Pan et al. (2013) established algorithms to derive the temporal patterns of phytoplankton community structure in the NSCS. Although these studies have provided valuable information for phytoplankton community structure in the NSCS, the temporal and spatial variations of the community structure in the NSCS as a whole still largely remains to be explored. In addition, comprehensive studies examining how chemical and physical factors interact with the variations of pigment distribution and phytoplankton community structure are also limited.

Here, we have determined the pigment composition in the euphotic zone of the NSCS for four cruises within three years, covering the coastal region, the continental shelf and slope, and the deep water basin. We have taken the advantage of this thematic study (NoSoCs) where many biogeochemical parameters were measured simultaneously, including major nutrient concentrations, basic hydrographic parameters, the abundance of *Pro*, *Syn*, and Pico, and temporal variations of climatology (Wong et al., 2015; Pan et al., 2015) to examine the environmental controls on the temporal and spatial variations of pigment composition and phytoplankton community structure in the region.

2. Material and methods

2.1. Sampling time and station

Pigment samples were collected during the following four cruises, June 2010, December 2010 to January 2011, December 2011, and late August to early September 2012. Detailed information of the sampling dates and time are shown in Table 1. Following the depth contour lines, the sampling stations are separated into four different coastal to offshore water transects numbered from the northeastern to the southwestern ends of the NSCS. The stations in order from offshore to inshore stations from T1 to T4 transects are 2 to 12, 25 to 13, 54 to 41, and 26 to 40, respectively (Fig. 1). The first cruise carried out in June 2010 covered all four transects. Due to the limitation of sampling time and severe weather in winter, the sampling stations of the 2nd cruise carried out in December 2010 were mainly located at T4 and the other four stations at T1 (Table 1). The cruises carried out in 2011 and 2012 were focused at T3, expending additional resources to study pigment distribution at a time series station, SEATS (Table 1). Samples were taken at SEATS for more than 30 h to study diurnal variations of pigment concentrations during the two cruises in 2011 and 2012 (Table 1).

2.2. Pigment sampling and analysis

Seawater samples for pigment analysis were collected by Go-Flo bottles mounted on a CTD rosette during every cruise. Two liters of seawater were transferred from Go-Flo bottles to 2.5 L dark bottles. Right after collection, the seawater samples were filtered on board through pre-combusted 47 mm Whatman GF/F filters under vacuum pressure of less than 100 mm Hg. The filters were preserved in tissue embedding cassettes and were kept frozen in liquid nitrogen until further processing in our land-based laboratory. In the land-based laboratory, the filters were first processed through freeze dryer for 24 h to remove water. Then the pigments in the filters were extracted by 90% acetone in the dark with sonication in an ice slurry for one hour. The extracted pigment samples were then filtered through a 0.2 μm PTFE syringe filter to remove particulate debris. The filtered extracted pigment samples were then ready to be analyzed. The pigments identified in the samples include mono-chlorophyll *a* (Chl *a*), fucoxanthin (Fuco), prasinoxanthin (Pras), alloxanthin (Allo), peridinin (Per), divinyl chlorophyll *a* (DV Chl *a*), chlorophyll b (Chl *b*), zeaxanthin (Zea), 19′•-hexanoyloxyfucoxanthin (Hex), 19′-but-fucoxanthin (But), chlorophyll *c2* (Chl *c2*), chlorophyll *c3* (Chl *c3*), lutein (Lut), neoxanthin (Neo), violaxanthin (Vio), diadinoxanthin (Diad), carotenes (Car), and diatoxanthin (Diat). Unabbreviated pigment names are listed in Table 2. The standards of Chl *a* and Chl *b* were purchased from Sigma Chemicals, and all other pigments were purchased from DHI (Denmark). The accuracy of the concentrations of Chl *a* and Chl *b* standards were periodically validated by UV–vis spectrophotometer (Shimatzu 1700) and fluorescence spectrophotometer (Hitachi F-7000).

We used both HPLC (Shimadzu LC-10A, Japan) and UPLC (Waters, ACQUITY, US) techniques for pigment analysis. The HPLC method was equipped with C18 column (Tosoh, 250×4.6 mm^2, particle size of 5 μm) by using ternary gradient elution procedures

Table 1
Sampling stations and times for all cruises. The first cruise (June 2010) covered four transects, the second cruise (December 2010) focused on transect T4, and the third and fourth (December 2011 and September 2012) cruises focused on transect T3.

Station	Date	Time	Station	Date	Time	Station	Date	Time	Station	Date	Time
2010_June											
26	6/4	21:11	42	6/6	15:15	25	6/3	15:01	12	6/11	12:07
28	6/5	7:10	44	6/6	16:38	23	6/8	14:39	10	6/11	13:48
30	6/5	11:38	46	6/6	19:36	21	6/10	16:19	8	6/11	16:16
32	6/5	15:32	48	6/6	22:53	19	6/10	20:33	6	6/11	19:13
34	6/5	18:05	50	6/7	2:57	17	6/11	0:00	4	6/11	22:28
36	6/5	20:47	52	6/7	8:15	15	6/11	2:28	2	6/12	12:04
38	6/5	22:07	54	6/7	16:14	13	6/11	3:36			
40	6/5	23:27									
2010_December–January			**2011_December**			**2012_August–September**					
2	12/30	10:05	41	12/21	3:46	SEATS	8/31	6:42			
26	12/31	22:40	42	12/21	5:38	SEATS	8/31	13:02			
27	6/1	5:23	43	12/21	7:27	SEATS	8/31	16:04			
28	1/1	10:08	44	12/21	9:18	SEATS	8/31	19:03			
29	1/1	14:43	45	12/21	11:18	SEATS	8/31	22:02			
30	1/2	13:09	46	12/21	14:30	SEATS	9/1	1:00			
32	1/3	1:02	47	12/21	16:39	SEATS	9/1	4:00			
34	1/3	6:24	48	12/21	19:47	SEATS	9/1	7:04			
38	1/3	13:54	49	12/21	22:44	54	9/1	23:35			
40	1/3	17:03	50	12/22	1:54	53	9/2	7:31			
12	1/6	5:01	51	12/22	4:55	52	9/2	11:24			
10	1/6	8:16	52	12/22	8:41	51	9/2	13:53			
8	1/6	12:58	53	12/22	18:59	48	9/2	6:59			
			54	12/23	1:38	45	9/2	23:31			
			SEATS	12/24	0:14	43	9/3	0:46			
			SEATS	12/24	5:02	41	9/3	1:56			
			SEATS	12/24	8:08						
			SEATS	12/24	10:59						
			SEATS	12/24	16:59						
			SEATS	12/24	20:10						
			SEATS	12/24	23:00						
			SEATS	12/25	5:02						
			SEATS	12/25	8:10						

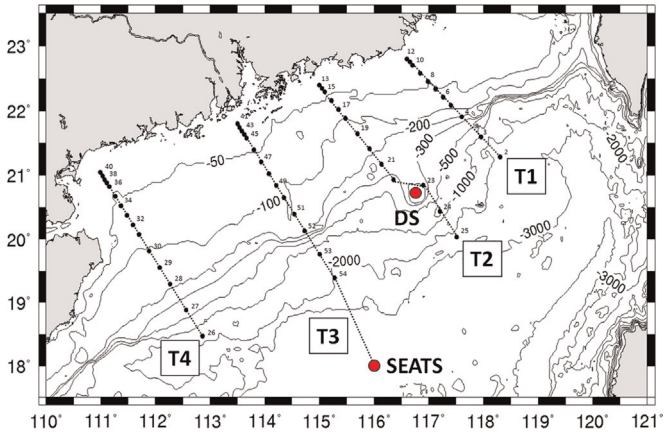

Fig. 1. The locations and station numbers in this study. The labeling T1, T2, T3, and T4 represent the four transects from the northeastern to southwestern ends in the studied region, respectively. The first cruise covered 4 transects, the second cruise mainly went to T4, and the 3rd and 4th cruises focused on T3. DS stands for Dongsha Atoll. SEATS, the time series station Taiwan has established since 1998, is located in the deep water basin (18°N, 116°E) of the NSCS. The detailed information of the sampling stations for each cruise is listed in Table 1.

Table 2
Pigments determined and their abbreviations used in this study.

Full name	Abbreviated name
Chlorophyll *a*	Chl *a*
Divinyl Chlorophyll *a*	DV Chl *a*
Divinyl Chlorophyll *b*	DV Chl *b*
Chlorophyll *b*	Chl *b*
Chlorophyll *c2*	Chl *c2*
Chlorophyll *c3*	Chl *c3*
Zeaxanthin	Zea
Fucoxanthin	Fuco
19'-hexanoyloxy-fucoxanthin	Hex
19'-but-fucoxanthin	But
Prasinoxanthin	Pras
Lutein	Lut
Peridinin	Per
Neoxanthin	Neo
Diadinoxanthin	Diad
Alloxanthin	Allo
Violaxanthin	Vio
Diatoxanthin	Diat
Carotenes	Car

(Mackey et al., 1996). This method does not differentiate DV Chl *a* from mono-Chl *a*. The total Chl *a* concentrations shown in this study are the concentrations obtained by the C18 column, which include both mono-Chl *a* and DV Chl *a* (Figs. 2–5). The three solvents used in this method included solvent A (80% methanol with 20% 0.5 M ammonium acetate at pH=7.2), solvent B (90% acetonitrile with 10% water), and solvent C (100% ethyl acetate), which were used in the following gradient program. The four numbers shown in the brackets include the time per minute set for each procedure and the relative percentages of solvents A, B, and C in mobile phase with the following five sequential steps: (0, 100, 0, 0), (4, 0, 100, 0), (18, 0, 20, 80), (21, 0, 100, 0), and (24, 100, 0, 0). The

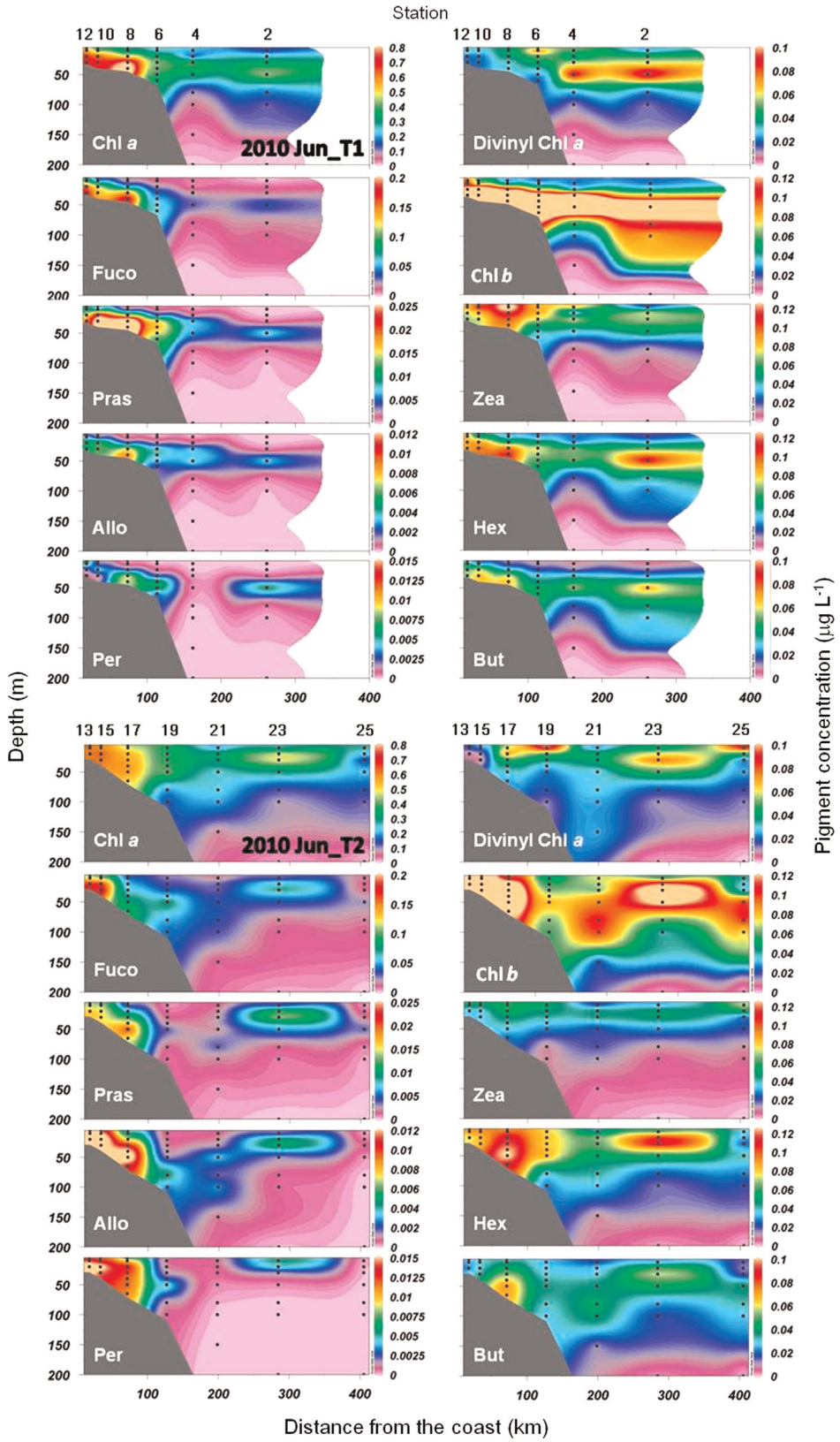

Fig. 2. The horizontal and vertical pigment concentrations and distribution at the stations of T1 and T2 in June 2010. The sampling depths are shown with black dots in the contours. For comparison between the two transects in the figures, we have adjusted the *x*-axis to be the same for the two transects. The numbers labeled on the top of the figures are the sampling stations. The concentration units for all colored bars are all $\mu g\ L^{-1}$. The scales are different among different pigments to exhibit the distribution features of every pigment. It should be noted that Chl *a* and Chl *b* concentrations shown from Figs. 2–5 are total Chl *a* and total Chl *b*, the sum of mono-Chl *a* and DV Chl *a* and the sum of mon-Chl *b* and DV Chl *b*, respectively. (For interpretation of the references to color in this figure legend, the reader is referred to the web version of this article.)

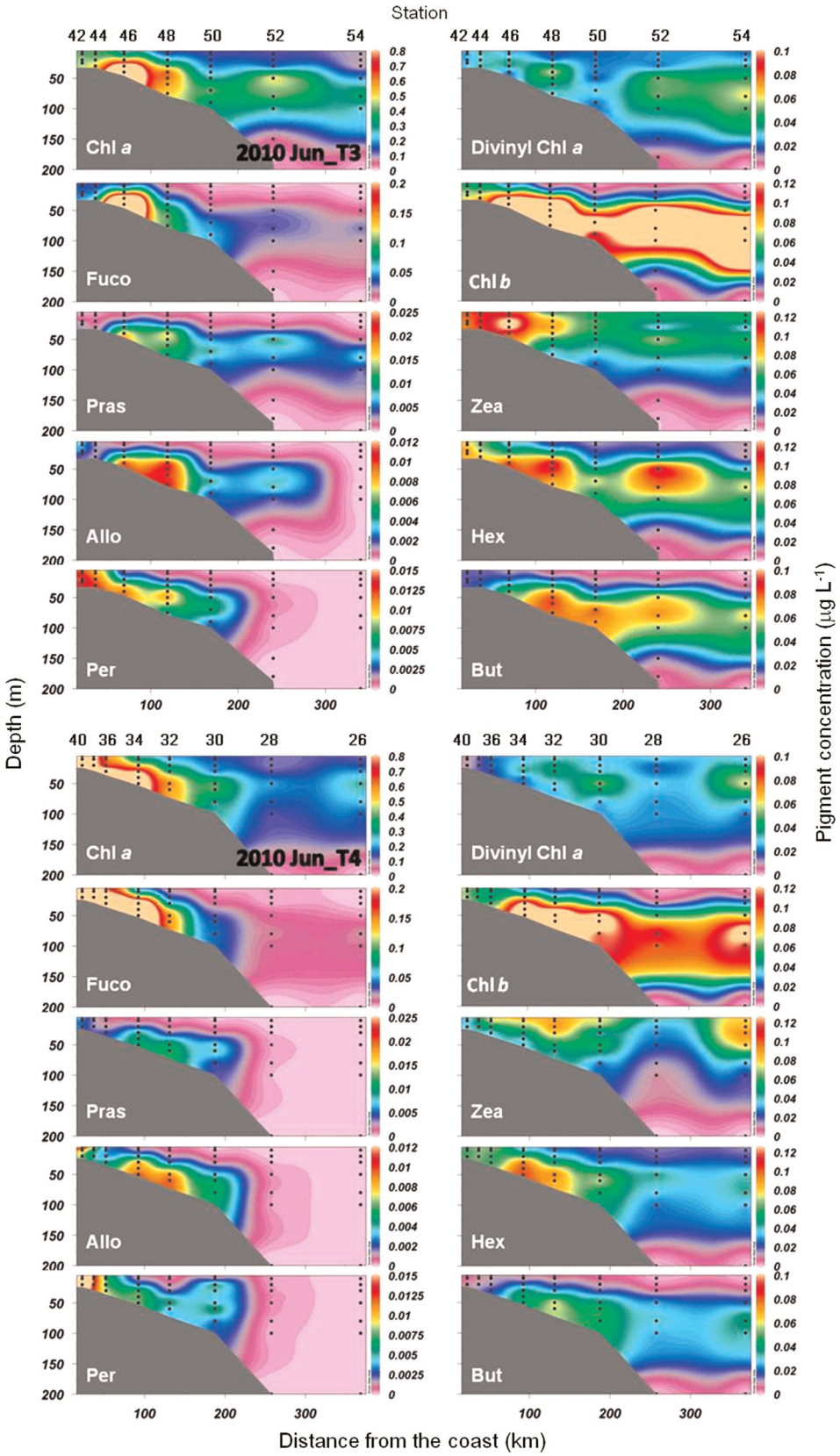

Fig. 3. The horizontal and vertical pigment concentrations and distribution at the stations of T3 and T4 in June 2010.

flow rate of the mobile phase was set to be 1 mL min^{-1} at 30 °C with UV–vis detection wavelength to be 436 nm. The UPLC method with C8 column (Waters, ACQUITY UPLC BEH C8, 2.1 × 150 mm^2, 1.7 μm) was mainly used for DV Chl *a* quantification. Modified from the recipe of Barlow et al. (1997), the mobile phases included solvent A (30% 1 M ammonium acetate with 70% methanol) and solvent B (100% methanol), which were mixed following these sequential gradient steps: (0, 30, 70), (2, 30, 70), (4, 0, 100), (5.5, 0,

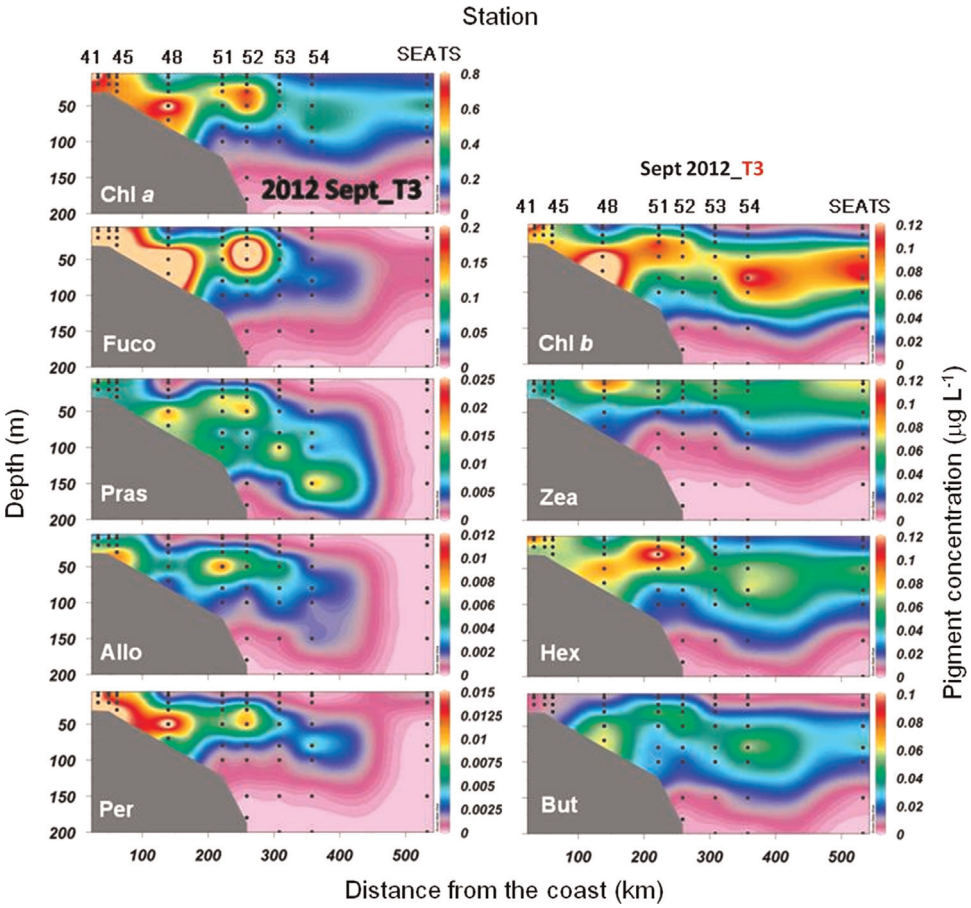

Fig. 4. The horizontal and vertical pigment concentrations and distribution at the stations of T3 in September 2012.

100), and (7, 30, 70). The samples were measured at 436 nm at 30 °C with a flow rate of 0.2 ml per minute. The data of the DV Chl *a* concentrations for the two latter cruises are not available due to system clogging issues. Other environmental parameters used in this study were sampled simultaneously as the pigment samples collected, which include basic hydrographic parameters, major nutrients, and the abundance of *Syn*, *Pro*, and Pico. The details of the methods used to determine these parameters are presented in detail in Wong et al. (2015).

The seasonal and spatial variations of the pigment distributions are presented as transect contour profiles to exhibit the vertical and spatial features (Figs. 2–5). Shown in Table 1, the June 2010 cruise was the only cruise that sampled in all four transects (Figs. 2 and 3). The results of Figs. 4 and 5 are transects T4, T3, and T3 from December 2010, December 2011, and September 2012, respectively. The sampling stations of T3 were surveyed on three cruises and T4 on two cruises. Due to limited space, only ten relatively abundant pigments are exhibited in the results (Figs. 2–5), including total Chl *a*, Fuco, Pras, Allo, and Per in the left panels and DV Chl *a*, Chl *b*, Zea, Hex, and But in the right panels (Figs. 2–5).

3. Results

3.1. Vertical and horizontal variations

The vertical and horizontal distribution of the pigment concentrations are presented via contour figures (Figs. 2–5). We have observed that some pigments possess elevated concentrations in the coastal region and some other pigments exhibit relatively high concentrations in the offshore region. To view the correlation of different pigment contour figures, we have thus arranged the contour figures into two panels for each cruise, with the left panel showing pigments with elevated concentrations in the coastal region and the right panel showing pigments with relatively elevated concentrations in the offshore region (Figs. 2–5). To simplify the description of the pigments in these two panels, we entitle the pigment group shown on the left panel as 'coastal type' pigments and the pigment group shown on the right panel as 'offshore type' pigments. As shown in figures (Figs. 2–5), significant interseasonal, intraseasonal, and spatial variations are observed for all of the pigments in the studied region. The maxima of the coastal type pigments were mainly located near the coast or near the bottom depth on the continental shelf, which exhibited elevated concentrations in the top 100 m within a 150 km distance from the coast. The off-shore type pigments tend to exhibit elevated concentrations for both the coast and the offshore regions. Overall, Chl *a* maxima were observed in the continental shelf region at depths shallower than 100 m for all transects in June 2010, with concentrations ranging from 0.50 to 1.20 μg L^{-1} (Figs. 2–5). In June 2010, the Chl *a* maximum value was located right above the continental sediments for transects T1, T3, and T4. In the offshore region, the maximum Chl *a* concentrations generally ranged from 0.10 to 0.40 μg L^{-1}. It should be noted that Chl *a* data shown in the figures include both normal Chl *a* and DV Chl *a* so that DV Chl *a* may account for a significant portion of the Chl *a* concentrations in the offshore water. The concentrations of total Chl *a* were elevated

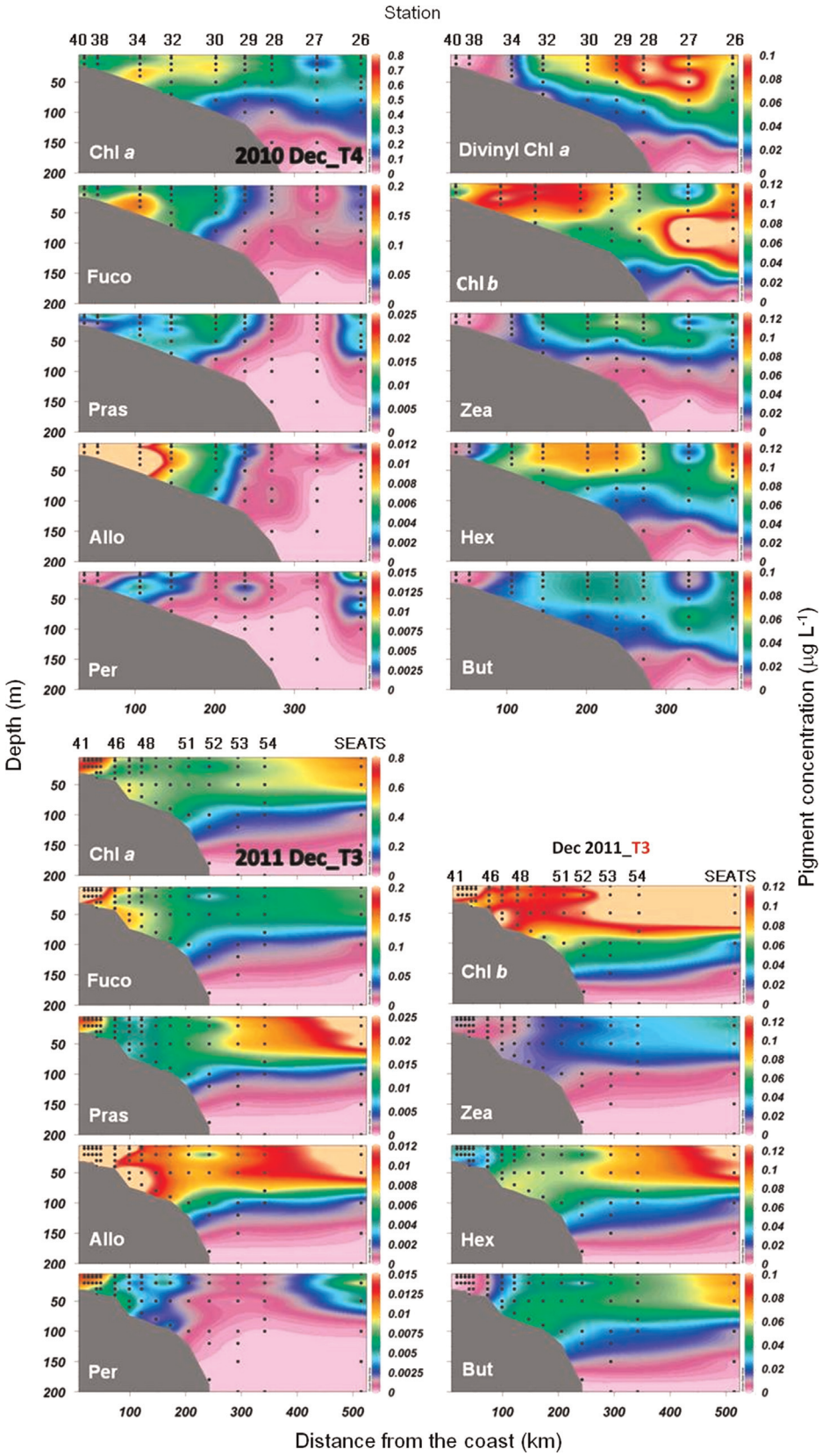

Fig. 5. The horizontal and vertical pigment concentrations and distribution at the stations of T4 December 2010 and T3 in December 2011.

and homogeneously distributed in the top 80 m of the offshore water for transect T2, where the offshore stations are close to Dongsha Atoll. The concentrations of Chl *a* reached 150 m in the two southern transects (T3 and T4) with relatively low value in the top 30 m. In September 2012, the Chl *a* maxima feature was extended from the coastal region to the offshore water. In the two

December cruises, the Chl *a* concentrations were significantly elevated in the offshore water and were relatively homogenously distributed in the whole transect (Figs. 2–5).

The concentrations of DV Chl *a* were determined in the samples collected in both June and December 2010 (Figs. 2, 3 and 5). Horizontally, the distribution of the maximum concentrations in the offshore water were comparable to total Chl *a* maximum depth, generally ranging from 0.05 to 0.20 μg L^{-1} where total Chl *a* generally ranged from 0.20 to 0.40 μg L^{-1}. Among the four transects of 2010, the DV Chl *a* concentrations obtained in the two northern transects, T1 and T2, were higher than T3 and T4. The concentration maximum depths at T1 and T2 were shallower than transects T3 and T4. DV Chl *a* and Zea were generally high from the water surface down to 150 m, from the coast to the offshore water (Figs. 2–4). Spatially, the concentrations of DV Chl *a* and Zea at the northern transects (T1 and T2) were significantly higher than the southern transects. Hex and But exhibited similar patterns vertically and horizontally. Chl *b* is a dominant pigment in both the coastal and offshore regions. The maxima concentrations of Chl *b* were located in the zone between 50 and 150 m, generally ranging from 0.10 to 0.30 μg L^{-1} (Figs. 2–5). The concentrations from 20 to 50 m were particularly low. During June 2010, Zea concentrations were relatively high in the top 100 m from the coastal to the offshore water, with concentrations ranging from 0.06 to 0.15 μg L^{-1}. The concentrations were particularly high for T1 and T3 in the coastal region within a 100 km distance from the coast. Similar concentrations and distribution patterns were also observed in September 2012. For the two winter cruises carried out in 2010 and 2011, Zea concentrations were also homogeneously distributed in the top 100 m and the concentrations were around 0.06 and 0.03 μg L^{-1}, which were significantly lower than the value observed in summer time. During the winter time, Zea concentrations in the coastal region decreased to 0.01 μg L^{-1}, most likely also influenced by the low temperature–low salinity coastal current (Pan et al., 2015).

Fuco showed a similar distribution pattern with Chl *a* in the coastal region (Figs. 2–5). Fuco maximum concentrations were up to 0.40 μg L^{-1} in the coastal and shelf regions for T3 and T4 in June 2010, showing that Fuco was a major phytoplankton pigment in the coastal region. In December 2010, the concentration maxima were observed right above the sediments in the shelf region and the elevated concentrations were extended to the shelf break. However, during December 2011, like most of the other pigments measured, Fuco concentrations were homogenously distributed in the continental and offshore water at T3 with concentrations around 0.10 μg L^{-1}.

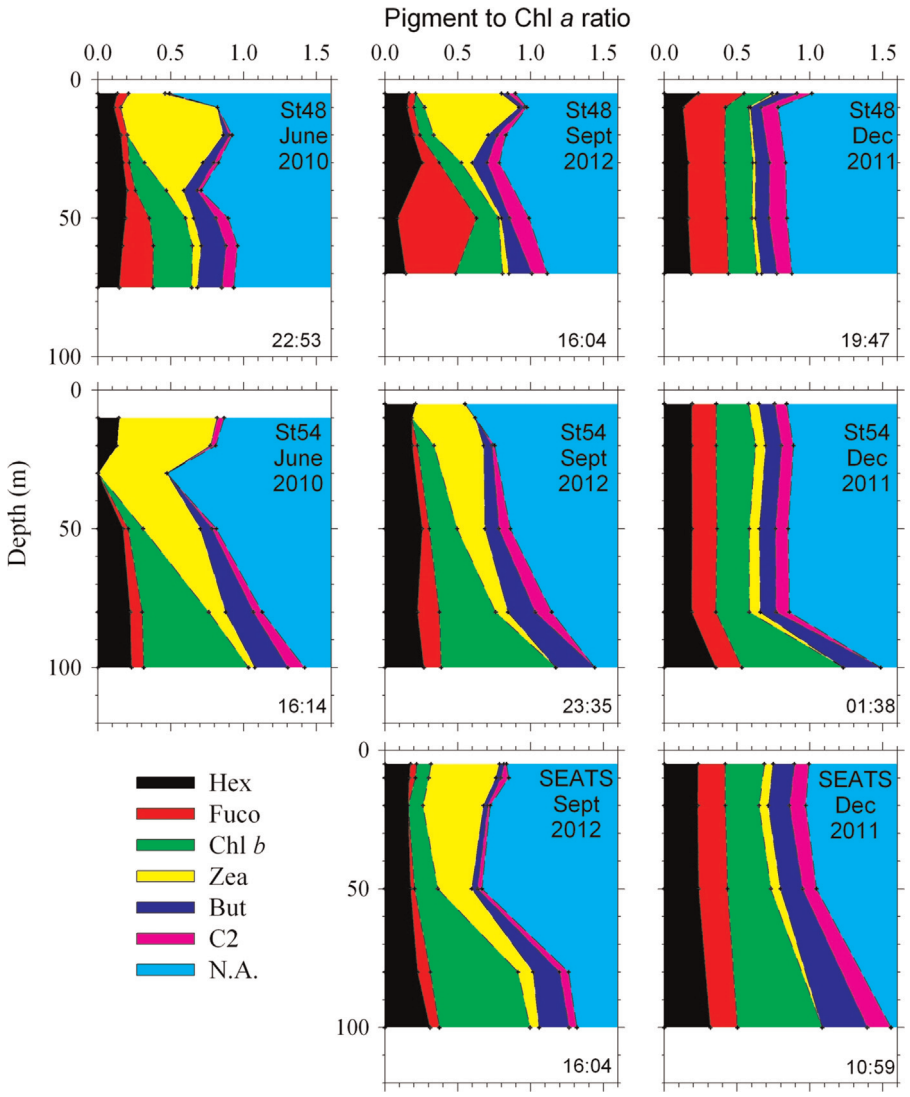

Fig. 6. The accumulative vertical profiles of pigment to Chl *a* ratios at stations 48, 54, and SEATS in June 2010, December 2011, and September 2012. The region with light blue background color and the cruise date information is not data. (For interpretation of the references to color in this figure legend, the reader is referred to the web version of this article.)

3.2. Vertical pigment ratios

The vertical variations of individual pigment to Chl *a* ratios are presented to illustrate the relative abundance of the marker pigments or semi-quantitatively the major phytoplankton groups in the NSCS (Fig. 6). Since we have carried out pigment measurements at transect T3 for three cruises we choose three stations at T3, a shelf station 48 and the other two deep water stations 54 and SEATS station as examples to show the seasonal and vertical variations of the pigments (Fig. 6). Similar vertical and seasonal patterns for all of the pigments were observed among all three stations (Fig. 6). For June 2010, Hex, Fuco, Chl *b*, Zea, But, and Chl *c2* are the major pigments both in the shelf and basin regions. Particularly, Zea accounted for 50% or more than 50% of accumulative value of the six pigments in the top 30 m. Zea percentage was highest in the top 20 m and quickly decreased to value less than 10% in the deeper water of the shelf station but gradually decreasing to the bottom depths for the two deep water stations (Fig. 6). In contrast to Zea, the pigments showing increased percentage with depths are Chl *b*, But, and *Pro*. The percentages of Chl *b* increased with depth from less than 5% in the water surface to 20–30% in the deeper depths at St 48 and the percentages were up 70% in the deeper water of the two basin stations. Fuco patterns are significantly different between the shelf and the basin stations, with increasing percentages with depths up to 20–30% in the bottom depth at the shelf stations but only accounting for 5–10% in the deep water at the basin stations, indicating the percentages decreased from the coast to the deep water. The vertical variation patterns of the pigments disappeared in the winter cruise. All of the pigments exhibited consistent percentages vertically from the shelf to the basin water in December 2011, with relatively high and constant percentages for Hex, Fuco, and Chl *b* from the water surface to 100 m (Fig. 6). Vertically, the strong winter monsoon homogenizes the surface water, the pigment distribution, and the phytoplankton community structure in the NSCS. Horizontally, Fuco percentage decreases with increasing distance from the coast and the relative percentages of Chl *b*, Hex, and But increase with increasing distance from the coast. Fuco percentage in the coastal region generally accounted for 20–50% of the total pigment value and decreased to 10% or less in the offshore water.

3.3. Temporal and diel variations

In the summer cruises, Chl *a* exhibited elevated values near the coast and the shelf regions (Figs. 2–8). The concentrations of the other coastal type pigments, including Fuco, Pras, Allo, and Per were also elevated in the near shore region (Figs. 2–5). Similar seasonal patterns were observed for samples collected at T3 in June 2010 and December 2011. In December 2011, the coastal type pigments show homogeneously elevated concentrations in the top 100 m from the coast to the offshore water with a similar distribution pattern as the offshore type pigments, including Chl *b*, Zea, Hex and But (Fig. 5). The results at T4 show that the concentrations of Chl *a*, DV Chl *a*, and Chl *b* were elevated in the offshore water during the winter time. The distribution of the pigment concentrations in September 2012 exhibits a pattern similar to the results obtained in June 2010 (Fig. 4). However, the coastal type pigments measured in September 2012 significantly extended from the coastal water to the offshore region (Fig. 4).

The interseasonal and intraseasonal variations of depth integrated Chl *a* among different transects and stations are shown in Fig. 7. The seasonal variations of the pigment distribution are available for T4 in June 2010 and December 2011 and are available for T3 in June 2010, December 2011, and September 2012. Overall, the integrated Chl *a* value ranged from 10 to 40 mg m^{-2}. The integrated Chl *a* value was relatively consistent among the four

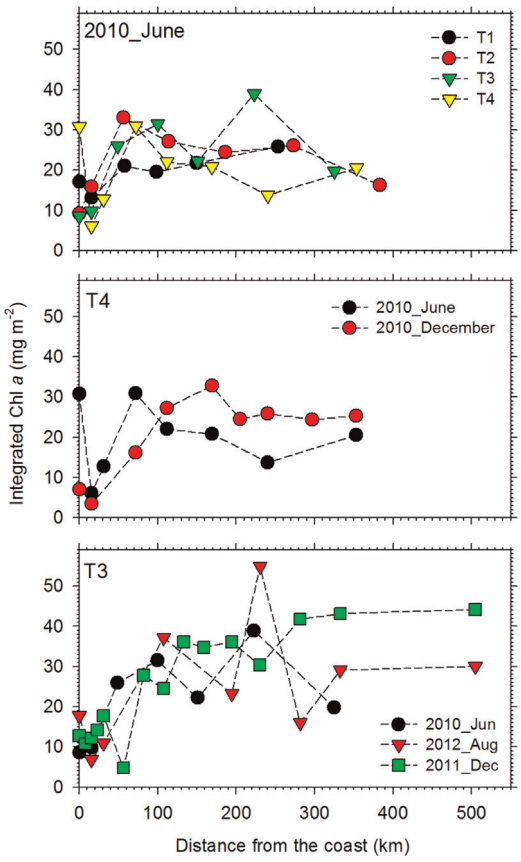

Fig. 7. Horizontal variations of integrated Chl *a* (mg m^{-2}) among different transects and seasons. The value is integrated down to the bottom in the coastal and the shelf regions or down to 200 m in the deep water stations.

transects in June 2012 (Fig. 7), ranging from 10 to 20 mg m^{-2} in the coastal water. High values at station 52 were observed for both summer cruises, where the topography gradient is high. The elevated value is related to relatively high biomass at the depth between 25 and 100 m. For the winter cruise, the integrated Chl *a* increased from 10 to 30 mg m^{-2} from the coastal zone to the offshore water, compared to the slightly lower value observed in the summer cruise. In the offshore water, the integrated Chl *a* values in the winters were about 20–50% higher than the value observed in the summer at the same stations.

In addition to seasonal variations, diel variations of Chl *a* concentrations at SEATS station were also studied in the cruises of December 2011 and September 2012 (Fig. 8). In terms of vertical variations, the Chl *a* concentrations were relatively low in the water surface in the September occasion, ranging from 0.05 to 0.15 μg L^{-1} in the top 20 m and were elevated to 0.30 ± 0.15 μg L^{-1} in the zone from 50 to 80 m. During December, the concentrations were 0.50 ± 0.15 μg L^{-1} in the top 50 m and the concentrations decreased with depths to 100 m (Fig. 8 top panel). The diel variations show that the highest and lowest pigment concentrations were observed in the late afternoon and midnight, respectively (Fig. 8). The diurnal patterns of integrated Chl *a* at SEATS station exhibited similar diurnal patterns for the two cruises (Fig. 8 bottom panel). The concentrations generally increased from 6 AM to 6 PM then decreased to a baseline at midnight then maintained relatively stable until to 6 AM. The variations of the diurnal Chl *a* values can reach two fold differences between early morning and late afternoon within 24 h at the same station. All other pigments exhibited similar diel patterns as Chl *a* so that their normalized value are relatively stable diurnally (Fig. 8). Light intensity appears to be a

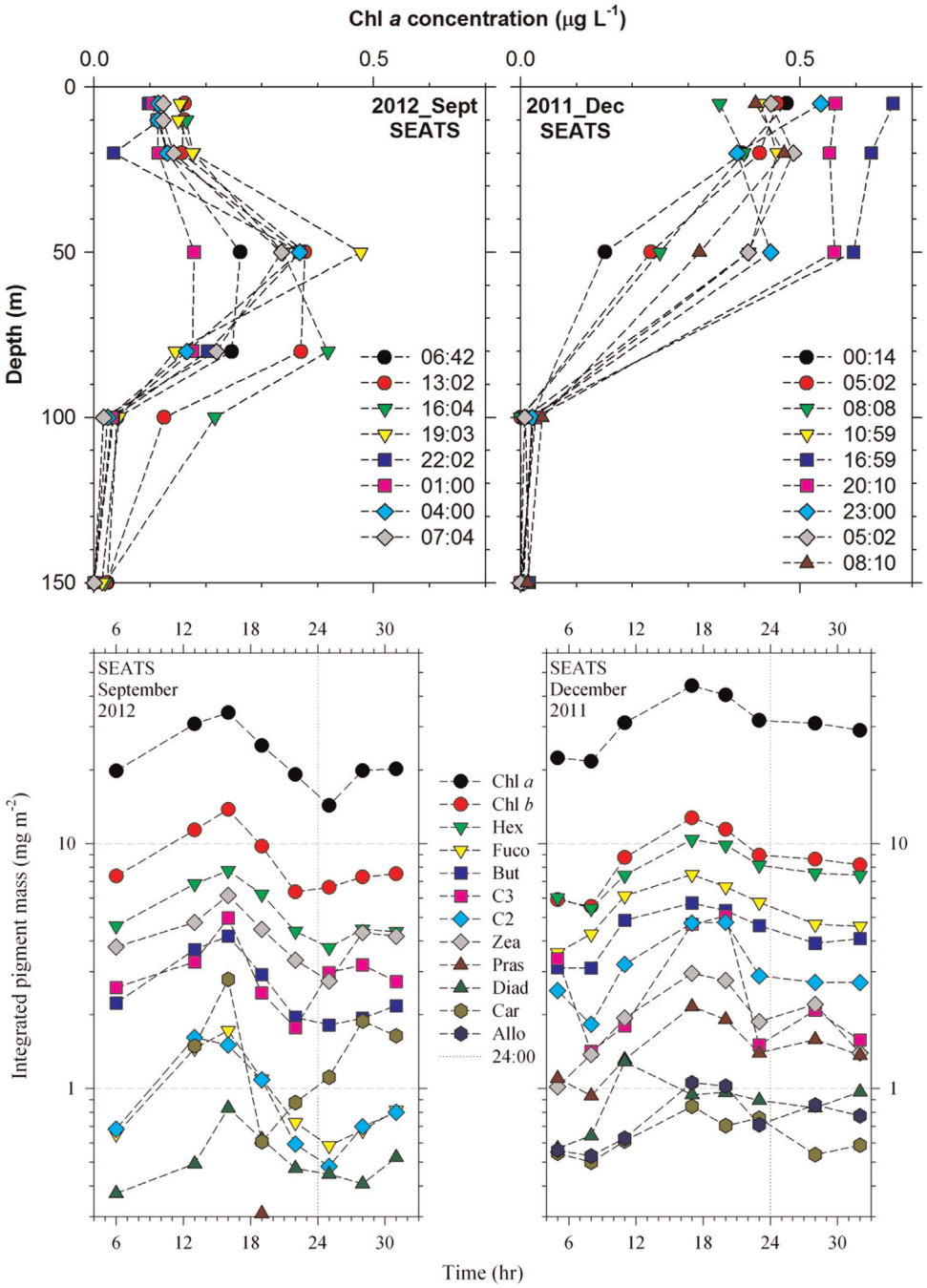

Fig. 8. The vertical and diel variations of Chl *a* concentrations (upper panel) and depth-integrated pigment mass (lower panel) obtained in September 2012 and December 2011 at SEATS station. The time information shown in the *x*-axis of the lower panel was the diel time scale.

major control on the diel variations. The results indicate that correction is needed for Chl *a* comparison for samples collected at a different time. The vertical and diel variations of the Chl *a* may prove useful in improving the method using satellite image for primary production estimate. The method uses Chl *a* data obtained from surface water light reflection to estimate phytoplankton biomass. Reflective signals of satellite images from the top few meters assume homogeneous Chl *a* concentrations in the mixing layer. Algorithms for using Chl *a* concentrations to estimate phytoplankton biomass should consider the variations of Chl *a* during different diurnal time or seasons to enhance the accuracy of the estimate in tropical and subtropical oceanic waters.

4. Discussion

4.1. Environmental controls on pigment distribution

Both bottom-up control by chemical and physical parameters and top-down control by grazing effect can be important factors in regulating phytoplankton abundance and pigment distribution in the marginal sea (e.g., Furuya et al., 2003). However, we only focus on bottom-up control here since the related study for top-down control was not available for this thematic study. In tropical marginal seas, temperature and light intensity are both relatively high. The temperature in the NSCS generally ranges from 20 to 30 °C in the top 50 m from winter to summer and the light intensity in the

water surface may reach up to 4000 μE m^{-2} s^{-1} at midday all year long. Major nutrient supply is thus most likely to be the major limiting factor for phytoplankton growth and becomes the major environmental factor controlling Chl *a* concentrations or phytoplankton abundance in the NSCS. However, using principal component analysis, the overall correlation between nutrient concentrations and pigment concentrations was extremely weak when all of the data was pooled together for statistical evaluation. We then examined the correlation between nutrients and Chl *a* concentrations first station by station, then region by region. During the two summer cruises, the elevation of the coastal type pigments was concentrated at the stations near the coast and/or right above the shelf sediments with bottom depth shallower than 100 m (Figs. 2–5). Using the data obtained on transects T3 and T4 in June 2010 as examples, the distribution patterns of the coastal type pigments and major nutrient concentrations in the whole transects differed. The correlation between pigment distribution and nutrient concentrations is generally significant in a relatively small studied region in summer seasons. For example, we observed that the nitrate concentrations at the coastal stations 42 and 44 at T3 were all below detection limit (0.3 μM) with salinity ranging from 33.67 to 33.69 from the surface to the bottom depths, indicating low riverine and nutrient input at the two coastal stations. Compared to their adjacent stations, the concentrations of the coastal type pigments at stations 42 and 44 were also relatively low (Fig. 3). In contrast to the nutrient and pigment relationship observed on T3, the nitrate concentrations at the coastal station 40 at T4 ranged from 15 to 2.3 μM with salinity ranging from 28.80 to 32.40 at 5–20 m, indicating high freshwater discharge and high major nutrient input in the coastal region. The elevation of the pigments shown in the left panel, particularly Chl *a* and Fuco, was attributed to the sufficient supply of major nutrients (Fig. 3). Thus, the close association between major nutrient availability and Chl *a* abundance generally exists in a well-constrained biogeochemical region, such as coastal regions where riverine discharge and coastal upwelling can be strong.

In addition to the coastal zone, the other pigment maximum zone was observed right above the sediments with bottom depths ranging from 30 to 100 m. Using T3 as an example, except Per, all other coastal type pigments exhibited maximum concentrations in the shelf water where nitrate and phosphate concentrations were also elevated at the deeper depths at stations 46 and 48 at T3, with nitrate concentrations at 0.2 and 1.5 μM, respectively. Similar elevated nutrient concentrations were observed at the shelf stations 36, 34, and 32 at T4, where the concentrations of various coastal type pigments were elevated. Tracing the concentration gradients of the elevated nutrients, the major nutrient supply in the region most likely originated from riverine discharge or the sedimentary input on the shelf. The sources of the nutrients may come from the discharge of the Pearl River and other local rivers in Guandong province, the submarine ground discharge or the diffusion of nutrients generated from early diagenesis process. In addition, some other physical forcings, such as wind stress and direction, Kuroshio intrusion, and eddy formation and origins (Huang et al., 2010; Du et al., 2013), are also important parameters to influence the nutrient transport and mixing strength. Overall, nutrient supply appeared to be closely associated with the distribution of the coastal type pigments during summer seasons.

We have observed significant intraseasonal variations for all of the pigments. Shown by the contour feature, the extension degree of the coastal type pigments to the offshore water among the two summer cruises was significantly different (Figs. 2–5). For June 2010, the distance and the depth of the extension scale of the coastal type pigments were much shorter than September 2012. In September 2012, all of the coastal type pigments were greatly extended to the offshore water horizontally and vertically, reaching 400 km away from the coast with elevated concentrations down to 100–150 m at T3 (Fig. 4), while the same pigments extended to 200 km in June 2012. For example, the marker pigment of dinoflagellates, Per, was extended to the offshore water in September 2012. We found that the extension of the pigments was associated with the supply and transport of major nutrients in the region, which originates either from riverine discharge and/or sedimentary input.

To examine the correlation between Chl *a* and major nutrient in the shelf and the deep water stations, temperature, salinity, and the concentrations of Chl *a* and major nutrients are compared for June 2010 and September 2012 by using the common shelf and offshore stations, 48 and 54, as examples to illustrate their relationship (Fig. 9). The concentrations of major nutrients and Chl *a* were both relatively low in the surface water in June 2010 and were elevated in the surface water in September 2011. In June 2010, using the representative offshore stations 2, 26, 48, and 54 as examples, nitrate was completely depleted when phosphate concentrations were low but still detected, suggesting that the major limiting factor was nitrogen not phosphorus in the June. In addition, the concentrations of Chl *a* increased with depth from water surface to 50–80 m in September 2012 (Fig. 9). The increasing vertical gradients of Chl *a* were closely associated with phosphate availability during the September occasion. The strong association between Chl *a* and phosphate concentrations was also observed at SEATS during the September occasion.

We then further examine overall nutrients-Chl *a* correlation in three confined regions separated by bottom depths, roughly representing coastal, shelf, and deep water regions because the sampling sites of this study covered various biogeochemical domains where nutrient concentrations varied vertically and horizontally (Fig. 10). It should be noted that nitrate concentrations were determined by using flow injection analysis with 1-cm flow cell and a detection limit around 0.3 μm in this study (Wong et al., 2015). This is because most of the low level nitrate concentration (<1 μm) may not be accurate enough for the comparison. In terms of silicate concentrations, we have only observed low silicate concentrations (<1 μm) in 4 coastal stations (10, 12, 38, and 40) in June 2010. For all other stations of all cruise cruises, the concentrations generally ranged from 2 to 10 μM in the euphotic zone of the coastal regions and 3 to 6 μM in the surface water of the shelf and deep water regions. The concentrations of silicate are relatively replete in comparison with nitrate and phosphate. Thus, silicate is unlikely to be the major limiting factor for diatom growth in almost all of the studied stations. Soluble reactive phosphate concentrations in the surface water were manually determined by using 10-cm quartz cell in colorimetry and a detection limit down to 5–10 nM or 0.005–0.010 μM in this study. Most of the phosphate concentrations observed in the surface water were indeed significantly higher than the detection limit (Fig. 10). The concentrations of Chl *a* were compated with phosphate in the top 40 m of all sampling sites by separating the data to three different bottom depths among different cruises. We observed strong correlation between soluble reactive phosphate and Chl *a* in the three zones during the two summer cruises (Fig. 10; Table 3). All of these results indicate that major nutrients, phosphate and most likely nitrate as well, are major environmental controls for the spatial variations of Chl *a* concentrations in the summer time of the NSCS.

Similar to the 2010 summer cruise, the top 50 m surface water was featured with relatively low salinity and detected nitrate concentrations for all of the sampling stations in T3 transect studied in September 2012. However, phosphate concentrations were below detection limit in the mixed layer of the deep water stations during the September occasion (Figs. 9 and 10). The close correlation between phosphate availability and Chl *a* concentrations

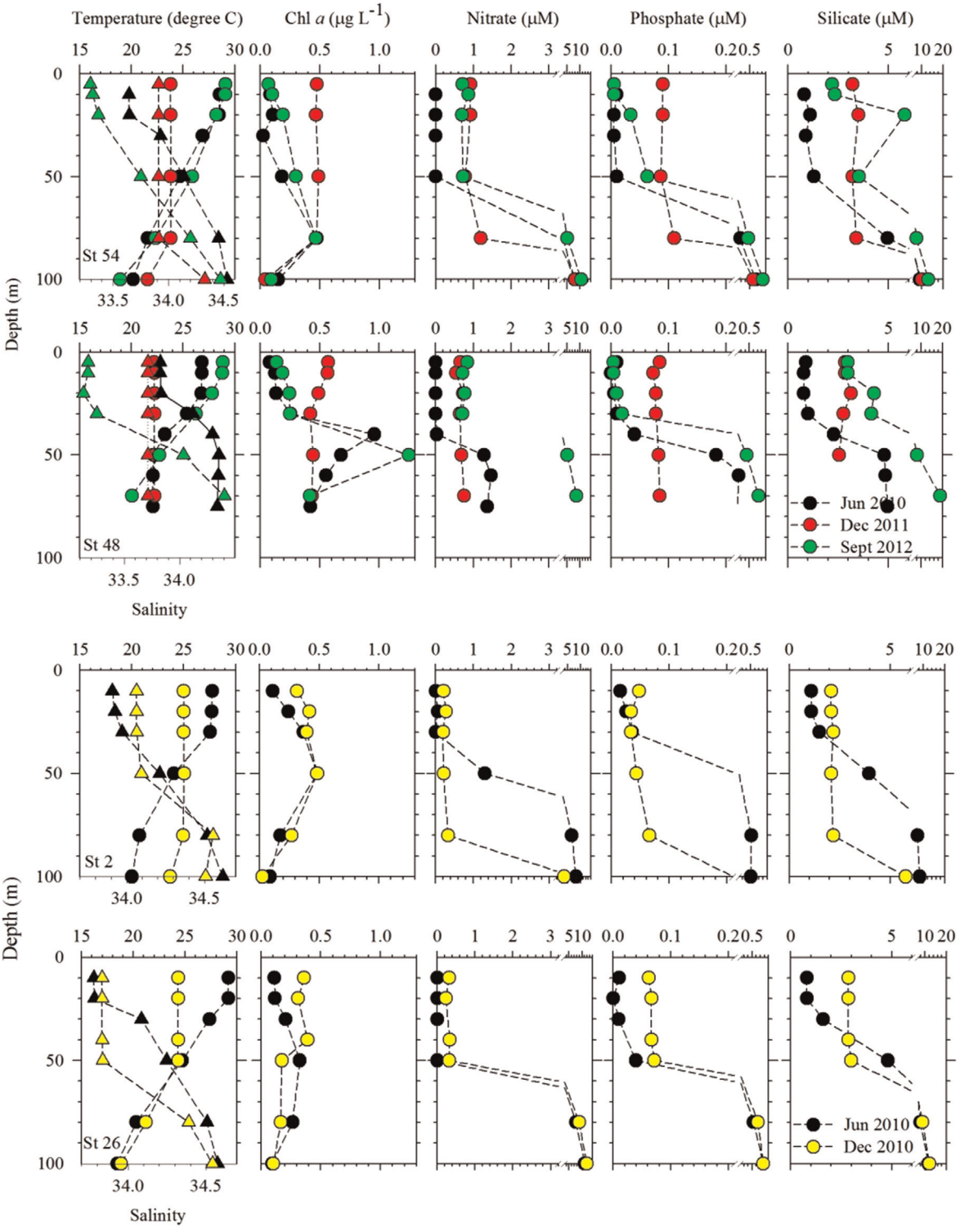

Fig. 9. The comparison of the vertical profiles of Chl *a* with temparature (circle), salinity (triangle), and major nutrients in the top 100 m at station 2, 26, 48, 54, and SEATS obtained in 2010 June (black), December 2010 (yellow), December 2011 (red), September 2012 (green). The detection limit of phosphate analysis in this study is much lower than nitrate. The details are shown in the discussion Section (4.1). (For interpretation of the references to color in this figure legend, the reader is referred to the web version of this article.)

observed in the September occasion (Table 3) suggests that P may become a particularly important limiting factor from early summer to late summer in the studied sites. The detected nitrate and low salinity surface water suggest that the input of terrestrial freshwater input might be the major source of the excess nitrate and could explain the extension of elevated coastal type pigments during the September occasion. The impact of the discharge may have important implications for the shift of phytoplankton community structure in the semi-closed SCS. The Pearl River discharge peaks in summer, which generally accounts for 50% of its annual discharge (http://www.mwr.gov.cn/; Pan et al., 2015). The August–September cruise took place at the end of the high discharge season and encountered the additional influence of riverine discharge. The discharge contains extremely high nitrate and

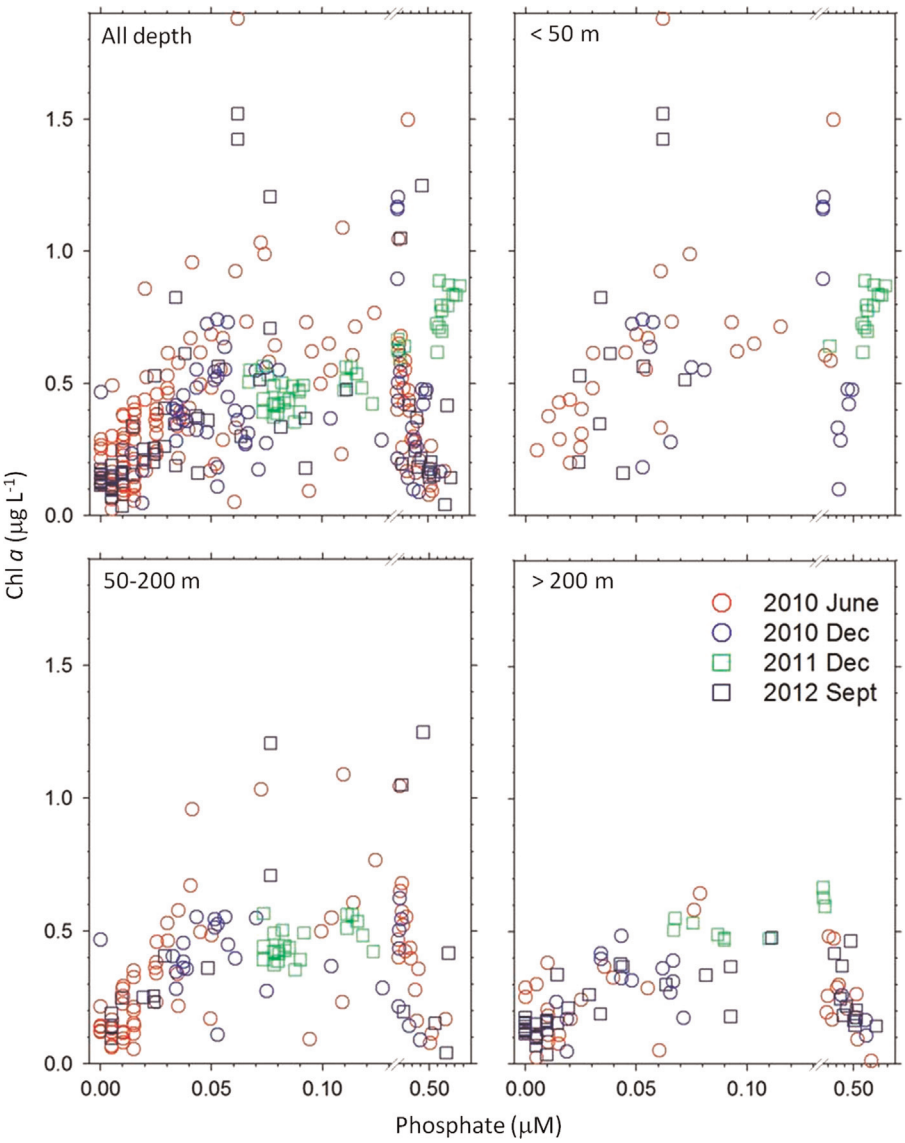

Fig. 10. The comparison of soluble reactive phosphate concentrations and Chl *a* concentrations. The top left figure include all data; the top right figure stands for the data collected at the stations with bottom depth shallower than 50 m. The bottom right and left figures stand for the data collected at the stations with bottom depth between 50 and 200 m and deeper than 200 m, respectively. The Chl *a* concentrations generally decreased with depth in most of the coastal and shelf stations. We thus emphasize on the concentration changes in the top 40 m by using breaks in the *x*-axis.

relatively low phosphate concentrations, ranging from 100 to 200 and 0.2–1 μM, respectively (Cai et al., 2004). Previous studies have reported excess nitrate and high alkaline phosphatase activities in the surface seawater of the coastal and the shelf region near the Pearl River during summer time, indicating excess nitrate and P limitation caused by the discharge (Yin et al., 2004; Xu et al., 2008; Huang, 2013). A similar phenomenon was also observed in the East China Sea (ECS), where the oceanic surface water exhibits low salinity, excess nitrate concentrations, and high alkaline phosphatase activities during summer time, also attributed to the impact of Changjiang discharge (Liu et al., 2013). The temporal variations of limiting nutrient status in the NSCS deserve long term observation. The techniques of low level nitrate and phosphate analysis are critical to identify the relative importance of nitrogen and phosphorus as limiting factors in the region.

The driving force of the nutrient supply to the euphotic zone is completely different during winter and early spring seasons in the NSCS. The mixing process driven by the winter monsoon appears to be the major factor elevating Chl *a* and primary production in the seasons of the NSCS (Chen, 2005; Tseng et al., 2005). The strength and length of the winter monsoon are expected to play a dominant role in controlling the vertical and horizontal variations of the pigment distribution in the NSCS during winter time. Indeed, we observed that the mixing process elevated nutrient concentrations in the surface water and resulted in homogeneous pigment distribution in the mixed layers (Figs. 3 and 4). It is expected that deeper mixing layers are the result of higher supplied nutrients. In December 2011, the nitrate and phosphate concentrations in the whole water column from stations 41 to 45 were up to 10 and 1 μM, respectively when the mixed layer was down to 100 m (Fig. 5). The concentrations in other deep water stations also reached 0.5–1.5 and 0.1–0.2 μM in the top 80 m. The nitrate to phosphate ratios in the water were all close to the Redfield ratio, indicating that the source of the nutrients originated from sub-surface water mixing. With lasting nutrient input by strong mixing in the euphotic zone, we observed that most of the pigments exhibited homogeneous distribution vertically from the coast to the offshore region (Fig. 5). The maximum pigment concentrations above the sediment observed in the summer became insignificant during the winter time. Relatively, we found

that the major nutrient concentrations and mixed layer depth at T4 stations in December 2010 were both much lower than the value obtained at T3 stations in winter 2011. In December 2010, the mixed layer depth was around 50 m for almost all of the stations at T4. The phosphate concentrations in the top 50 m of offshore stations 27 and 28 were down to 0.01–0.02 and 0.03–0.04 μM, respectively and the nitrate concentrations were around 0.30 μm. These relatively low nutrient concentrations in the surface water at the stations of T4 during the 2010 winter cruise may be attributed to relatively weak winter monsoon strength at this most southern transect by comparison with the elevated concentrations observed in December 2011.

It is known that low temperature coast current can be transported to the coastal region of the NSCS, mainly driven by winter monsoon (Jan et al., 2002; Pan et al., 2015). During the two winter cruises, relatively low salinity and temperature were observed in the coastal stations (Pan et al., 2015). We found that the low salinity low temperature coastal current transported from the Taiwan Strait remarkably influenced or replaced the phytoplankton community in the coastal and shelf regions of the NSCS. The concentrations of the offshore type pigments (e.g., Zea, Hex, But) significantly decreased in the coastal zone (Fig. 5). The NSCS is also a known oceanic region that encounters strong internal waves (Lien et al., 2005). The coupling effect of the waves and shallow submarine topography can be an important process to elevate nutrient concentrations regionally in the NSCS. The waves cause vertical advection and mixing and result in the elevation of major nutrients and Chl *a* concentrations in the surface water. We observed elevated concentrations for both major nutrients and Chl *a* concentrations at station 23 in T2, located right at the north end of the Dongsha Atoll (Fig. 1). In addition to the station near Dongsha Atoll, the concentrations of Chl *a* and other pigments were particularly high at station 52, both in June 2010 and September 2012 seasons. Station 52 is located right at the edge of the continental shelf margin, where the depth drops sharply from 200 m to 1000 m. We observed that the temperature at 100 m from stations 54 to 51 to be 18.92, 18.22, 18.10, and 19.61, suggesting that a weak upwelling process occurred in the subsurface water near the station.

Table 3
The correlation analysis of phosphate and Chl *a* concentrations in the three zones of the studied sites. We separate the sampling stations into three regions by bottom depths, less than 50 m, 50–200 m, and deeper than 200 m, respectively. The statistical parameters shown include correlation coefficient (r^2), significance probability (p), and observed sample number (n). Data processed only includes the samples collected at depths shallower than 50 m due to the limitation of light in the deeper depths (Fig. 11). The underlined numbers stand for the significant correlation ($p < 0.05$) between phosphate and Chl *a* in the regions.

Cruise time	Statistical parameter	Coastal (< 50 m)	Shelf (50–200 m)	Deepwater > 200 m
2010 June	r^2	0.51	0.36	0.38
	p	<u>< 0.001</u>	<u>< 0.001</u>	<u>0.003</u>
	n	56	50	21
2012 September	r^2	0.29	0.8	0.29
	p	0.11	<u>< 0.001</u>	<u>0.002</u>
	n	10	11	30
2010 December	r^2	0.12	0.04	0.38
	p	0.15	0.42	0.08
	n	18	19	9
2011 December	r^2	< 0.01	0.10	0.64
	p	0.98	0.18	0.06
	n	15	15	6

4.2. DV Chl *a* and zeaxanthin

Spatially, DV Chl *a* concentrations in the deep water region generally decreased from the northern to southern transects in June 2010 (Figs. 2–5). The spatial variations may be associated with the input of the Kuroshio water since *Pro* is known to be the dominant phytoplankton in the Kuroshio water (Wu and Hsin, 2012). Vertically, DV Chl *a* concentrations can reach 150 m deep in the offshore water, showing that *Pro* was a major phytoplankton group in the depth deeper than 100 m. Elevated DV Chl *a* concentrations in the offshore water were observed for T4 in December 2010, with concentrations up to 0.10 μg L^{-1} in the offshore region. The maximum zone of the DV Chl *a* was located in the top 100 m, particularly at stations 26 to 29. The cause for the elevation of DV Chl *a* relating to the increasing intrusion of Kuroshio water during winter time remains to be explored. DV Chl *a* concentrations were relatively low in the coastal water both in June and December.

Strong linear correlations are observed between DV Chl *a* and *Pro* abundance (Fig. 11). During the summer cruise, we found that two different slopes are observed in the upper and lower layers of

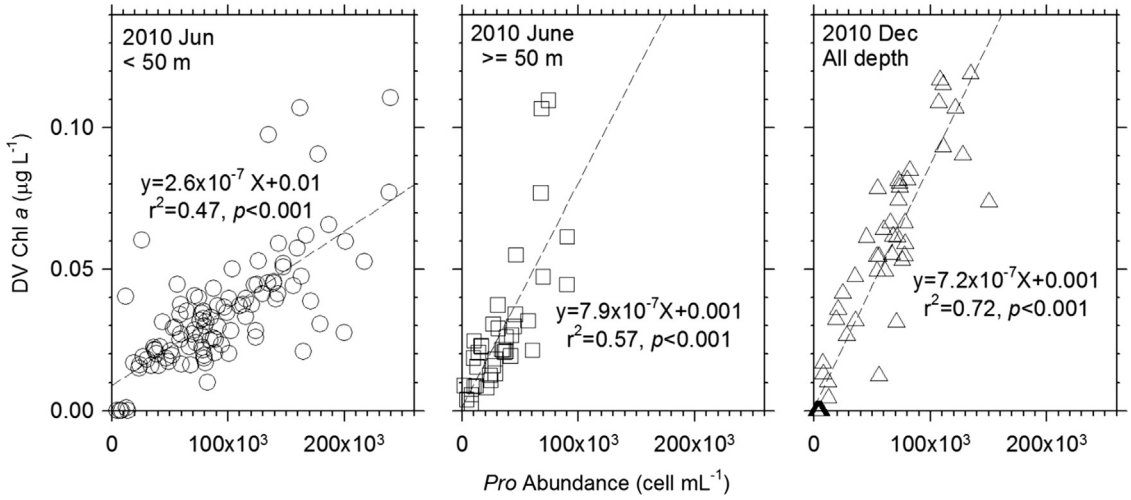

Fig. 11. The correlation between DV Chl *a* concentrations with *Pro* abundance among different cruises. It should be noted that the 2010 June data are separated into two layers, the top 50 m data and the data below 50 m, which is not related to bottom depths. The 2010 December data are all pooled together. The linear equation, correlation coefficient (r^2), and probability value (p) are shown in the figures.

all sampling stations, with slopes at 0.26 and 0.79 fg cell^{-1} for sampling depths shallower than 50 m and deeper than 50 m, respectively (Fig. 11). These ratios, comparable to the ratios reported previously for *Pro* (Moore et al., 1995), may be useful background information to differentiate high-light or low-light adapted ecotype *Pro* in the NSCS by DV Chl *a* and DV Chl *b* ratios. During the winter cruise carried out in 2010, we found that the concentrations of the pigment and the *Pro* abundance were both close to zero in all of the coastal stations, including stations 8, 10, and 12 of T1 and the 34, 38, and 40 of T4. The low temperature and low salinity southbound coastal current from the ECS brought low temperature and low salinity water with specific phytoplankton groups down to the coastal region of the SCS, which may explain the extremely low concentrations of DV Chl *a* and other offshore type pigments in the coastal region during winter time. In the December cruise, the cellular concentration was 0.72 fg cell^{-1}, similar to the value observed in the deeper layer in June 2010, indicating that the *Pro* observed in the December was likely to be dominated by the deep water strain observed in the summer.

Zeaxanthin exists in the groups of cyanobacteria, prasiophytes, and chlorophytes. *Syn* is known to be a major phytoplankton group in the NSCS (Cai et al., 2007; Chen et al., 2011). In addition, Zea concentrations in *Syn* are one order of magnitude higher than the Zea concentrations in prasiophytes and chlorophytes (Mackey et al., 1996; Lewitus et al., 2005). Although *Pro* also possesses Zea, the distribution patterns of Zea were significantly different from DV Chl *a* (Figs. 2 and 3). The maxima of Zea concentrations generally appeared in the surface water of the coastal region. These results indicate that Zea mainly originated from *Syn* in the coastal region so that Zea may be used as a marker pigment for *Syn* abundance in the coastal region of the NSCS. Indeed, we observed strong linear relationship between *Syn* abundance and Zea concentrations for three cruises (Fig. 12).

In June 2010, we found that Zea to *Syn* abundance ratios may be separated into two categories based on the bottom depths of sampling stations, including stations with bottom depth shallower than 100 m and offshore stations with bottom depths deeper than 100 m (Fig. 12). The ratios are 2.2 and 0.68 fg cell^{-1} for the deep and shallow regions, respectively. Since Zea is photoprotective pigment, it is expected to observe elevated pigment to *Syn* ratios in the offshore water stations during summer time. In December, Zea showed much lower abundance in the coastal region with bottom depth shallower than 100 m than the concentrations observed in June 2011. However, in September 2012, both Zea and *Syn* abundance were relatively low at all stations of T3 and did not show significant correlation either with or without depth separation ($r^2 < 0.1$, $p > 0.05$). For the two December cruises, similar to DV Chl *a*, the ratios are relatively consistent in all of the shallow and deep water stations, with the ratios to be 0.92 and 1.0 fg cell^{-1} for December of 2010 and 2011, respectively. The cellular Zea ratios appear to be seasonally and vertically specific, most likely to be controlled by light intensities. The pigment ratios are useful to estimate *Syn* abundance in the NSCS. Due to the large spatial and temporal variations of Zea concentrations per *Syn* cell, it is unrealistic to use single Zea to Chl *a* ratio to estimate cell abundance in the whole studied sites of the NSCS among different seasons.

Previous studies in the NSCS argued that *Pro* abundance was generally lower in winter time than summer time (e.g., Cai et al., 2007; Chen et al., 2011). In this study, we found that seasonal patterns of DV Chl *a* and *Pro* abundance are location specific in the NSCS. We did observe relatively low DV Chl *a* and Zea concentrations and relatively low *Pro* and *Syn* abundance in the areas of the coastal zone influenced by the cold coastal current during the winter time. In terms of offshore water, our study also observed that both DV Chl *a* concentrations and *Pro* abundance

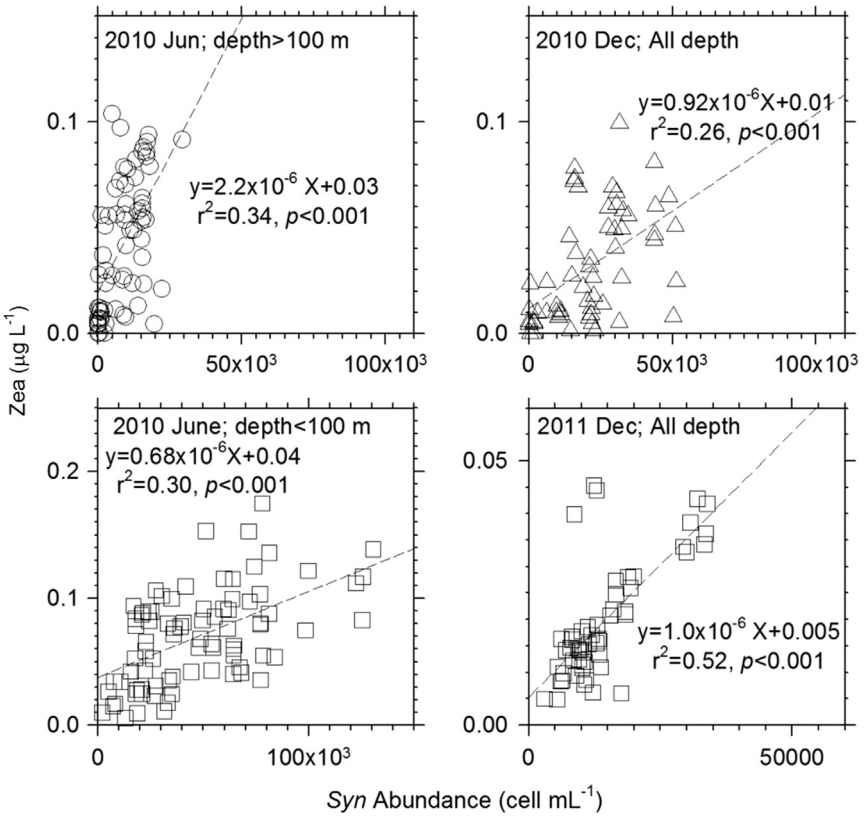

Fig. 12. The correlation between Zea concentrations and *Syn* abundance among different cruises. The 2010 June data are separated into two categories, with bottom depth shallower and deeper than 100 m. The December data are all pooled together without the separation.

varied significantly among different transects (Fig. 2). For example, the DV Chl *a* and *Pro* abundance were much higher in winter than summer at the deep water stations of T4 (Figs. 2–5). It should be noted that the influenced region by the winter coastal current may vary year from year or month from month in winter based on the fluctuations of the climatology in the region (Pan et al., 2015). Temperature does not necessarily results in a cause and effect relationship on the abundance of *Syn* or *Pro* in the region even though the correlation between temperature and cell abundance may be significant. Overall, the abundance of *Pro* and *Syn* and their corresponding pigments vary significantly among different seasons and locations in the NSCS.

4.3. Hex, But, and Fuco

Pigment Hex, a major pigment in the NSCS, exists in both haptophytes and dinoflagellates (Mackey et al., 1996; Zapata et al., 2004). In the offshore water, the Hex maximum concentrations were up to 0.10 μg L^{-1} and the major marker pigment of dinoflagellates, Per, were generally less than 0.01 μg L^{-1} or undetected in the offshore water (Figs. 2–5), indicating that Hex was mainly derived from haptophytes and was a specific pigment reflecting coccolithophore abundance in the offshore water of the NSCS. In the coastal water, although Per concentrations were slightly elevated to 0.01–0.02 μg L^{-1}, they were still much lower than Hex concentrations observed in the coastal region (Figs. 2–5). Overall, Hex is a marker pigment for haptophytes in the NSCS from the coastal to the offshore water.

During the two summer cruises, the distribution patterns of Hex were similar to Chl *a*, suggesting that nutrient supply was also the major control on the spatial variations. The Hex concentrations in the coastal region were elevated in the coastal water, ranging from 0.10 to 0.20 μg L^{-1}. In the offshore water, the maximum depth of Hex generally located at the depths from 50 to 100 m. Similar to the distribution of Chl *a*, the maximum depths were deeper at the stations of T3 and T4 and were shallower at the stations of T1 and T2. During the two winter cruises, elevated Hex concentrations were homogenously distributed in the top 100 m, the mixed layer in the outer shelf region of the deep basin water (Fig. 5). The Hex concentrations at SEATS station reached 0.15 μg L^{-1} in December 2011, indicating that strong mixing driven by winter monsoon also significantly enhanced coccolithophore abundance during winter time. The Hex concentrations in the coastal water during the two winter cruises were much lower than the value observed in summer time.

Significant linear correlations between pico-eukaryotes and Hex observed for all of the cruises further support the notion that haptophytes are major pico-eukaryotic phytoplankton in the NSCS during both summer and winter seasons (Fig. 13). Similar to Zea distribution, we found that the ratios of Hex to Pico abundance may be separated into two categories based on the bottom depths ($<$ or $>$ 100 m) of the sampling stations in 2010 summer (Fig. 13). The ratios are 13 and 6.5 fg $cell^{-1}$ for the deep and shallow regions, respectively (Fig. 13). As shown in the figure, the abundance of other groups of Pico (e.g., diatom) in the coastal region was higher in the coastal water and accounted for a higher percentage in the coastal water than the offshore water in the summer time, which may partially explain the relatively low ratios observed in the coastal stations. In the two December cruises, the ratios are 9.0 and 12 fg $cell^{-1}$ for 2010 and 2011, respectively. The highest Hex to Pico abundance ratio, observed in the 2012 September cruise, was up to 18 fg $cell^{-1}$, indicating that the percentage of coccolithophores was relatively high during the occasion. Similarly, using a molecular biology approach, Wu et al. (2014) reported that coccolithophores may account for up to 50% of Pico abundance in the NSCS in January 2010. Future studies to simultaneously measure coccolithophore abundance and Hex concentrations are needed to establish specific Hex to Chl *a* ratios for coccolithophores in the NSCS.

The other major marker pigment observed in the studied sites was But, a pigment only found in haptophytes and chrysophytes.

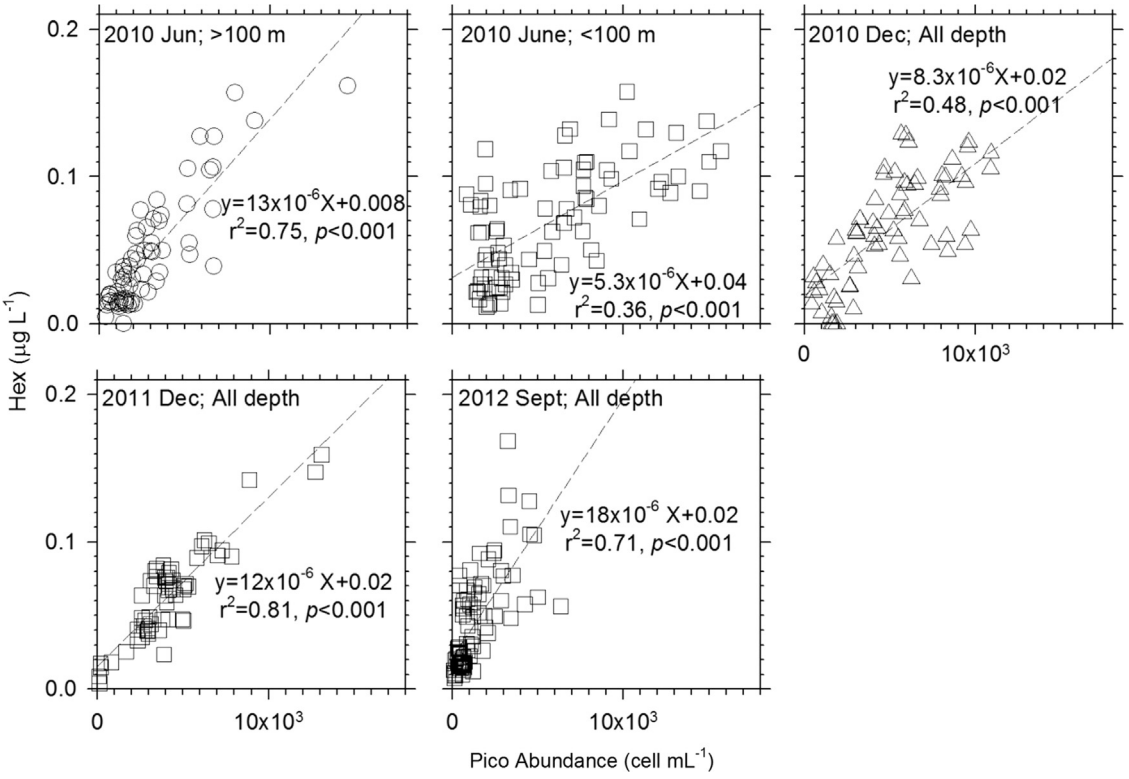

Fig. 13. The correlation between Hex concentrations and Pico abundance among different cruises. The 2010 June data are also separated into two categories, with bottom depth shallower and deeper than 100 m. The December data are all pooled together without the separation.

Table 4
The overall concentration correlation (r) among pigments in the four cruises.

2010 June	Chl *c3*	Chl *c2*	But	Fuco	Hex	Pras	Diad	Allo	Zea	Chl *b*	Chl *a*	Car
Chl *c3*	1.00											
Chl *c2*	0.80	1.00										
But	0.35	0.30	1.00									
Fuco	0.74	0.95	0.19	1.00								
Hex	0.48	0.44	0.77	0.29	1.00							
Pras	0.51	0.48	0.68	0.39	0.70	1.00						
Diad	0.70	0.89	0.30	0.84	0.59	0.46	1.00					
Allo	0.48	0.51	0.55	0.47	0.66	0.73	0.52	1.00				
Zea	−0.06	−0.09	−0.14	−0.15	0.15	0.05	0.15	−0.10	1.00			
Chl *b*	0.45	0.45	0.90	0.35	0.78	0.80	0.44	0.66	−0.07	1.00		
Chl *a*	0.77	0.93	0.44	0.91	0.62	0.62	0.91	0.62	0.07	0.60	1.00	
Car	0.59	0.65	0.51	0.57	0.75	0.65	0.75	0.52	0.39	0.69	0.82	1.00

2010 Dec	Chl *c3*	Chl *c2*	But	Fuco	Hex	Pras	Diad	Allo	Zea	Chl *b*	Chl *a*	Car
Chl *c3*	1.00											
Chl *c2*	0.73	1.00										
But	0.24	−0.07	1.00									
Fuco	0.49	0.90	−0.32	1.00								
Hex	0.65	0.70	0.53	0.49	1.00							
Pras	0.27	0.23	0.31	0.01	0.35	1.00						
Diad	0.58	0.88	0.03	0.78	0.75	0.30	1.00					
Allo	0.36	0.77	−0.47	0.86	0.24	0.04	0.58	1.00				
Zea	0.14	0.00	0.61	−0.25	0.48	0.27	0.19	−0.37	1.00			
Chl *b*	0.46	0.64	0.41	0.53	0.72	0.25	0.64	0.39	0.10	1.00		
Chl *a*	0.61	0.94	−0.05	0.90	0.73	0.18	0.87	0.77	0.12	0.65	1.00	
Car	0.53	0.48	0.59	0.26	0.77	0.23	0.55	0.13	0.71	0.60	0.59	1.00

2011 Dec	Chl *c3*	Chl *c2*	But	Fuco	Hex	Pras	Diad	Allo	Zea	Chl *b*	Chl *a*	Car
Chl *c3*	1.00											
Chl *c2*	0.40	1.00										
But	0.56	−0.32	1.00									
Fuco	−0.11	0.79	-0.71	1.00								
Hex	0.68	0.08	0.88	−0.38	1.00							
Pras	0.23	0.54	0.07	0.41	0.37	1.00						
Diad	0.12	0.66	−0.31	0.69	−0.01	0.35	1.00					
Allo	−0.16	0.68	−0.61	0.81	-0.30	0.41	0.59	1.00				
Zea	0.41	−0.03	0.71	−0.34	0.82	0.48	−0.04	−0.17	1.00			
Chl *b*	0.44	0.61	0.18	0.28	0.53	0.58	0.26	0.24	0.52	1.00		
Chl *a*	0.12	0.88	−0.44	0.92	−0.03	0.61	0.77	0.80	0.01	0.52	1.00	
Car	0.02	0.60	−0.37	0.71	−0.04	0.47	0.55	0.63	0.20	0.49	0.81	1.00

2012 Sept	Chl *c3*	Chl *c2*	But	Fuco	Hex	Pras	Diad	Allo	Zea	Chl *b*	Chl *a*	Car
Chl *c3*	1.00											
Chl *c2*	0.93	1.00										
But	0.62	0.52	1.00									
Fuco	0.94	0.97	0.46	1.00								
Hex	0.57	0.55	0.80	0.46	1.00							
Pras	0.67	0.68	0.56	0.68	0.55	1.00						
Diad	0.19	0.39	0.08	0.35	0.41	0.24	1.00					
Allo	0.48	0.53	0.35	0.49	0.45	0.62	0.20	1.00				
Zea	−0.09	−0.06	−0.27	−0.08	0.08	−0.20	0.24	−0.26	1.00			
Chl *b*	0.51	0.39	0.89	0.33	0.76	0.38	0.11	0.38	−0.28	1.00		
Chl *a*	0.90	0.91	0.62	0.89	0.77	0.66	0.45	0.50	0.13	0.55	1.00	
Car	0.48	0.46	0.42	0.44	0.33	0.53	0.15	0.09	0.01	0.32	0.45	1.00

The But to Hex concentrations show a strong linear correlation for all cruises (Table 4). The But to Hex concentration ratios are 0.50, 0.32, 0.47, and 0.52 from the 2010 June to the 2012 September cruise. Aside from the relatively low ratio observed in 2010 December, all other ratios are almost identical to But to Hex ratios reported for haptophytes in previous studies, which is 0.50 (e.g., Mackey et al., 1996). Since Hex in the NSCS was mainly derived from haptophytes, the 0.5 ratios observed in the NSCS suggest that But might mainly come from coccolithophores. The consistent and comparable But to Hex ratios also suggest that chrysophytes are unlikely to be a dominant phytoplankton group in the NSCS.

Pigment Fuco is found in three major phytoplankton groups, bacillariophytes (diatom), haptophytes (coccolithophores), and cryptophytes (Mackey et al., 1996). Overall, the distribution pattern of Fuco observed in the NSCS behaved like Chl *a*, with elevated values in the coastal region and above the shelf sediments, decreasing with increasing distance from the coast. Because Fuco significantly and linearly correlated to pigment Chl *c2* (Fig. 14), the ratios are 0.23, 0.21, 0.18, 0.29 from 2010 June to 2012 Sept cruises, respectively. These ratios are also close to the Chl *c2* to Fuco ratios reported previously (Mackey et al., 1996; Zapata et al., 2011), indicating that both Fuco and Chl *c2* mainly come from diatoms. In addition, Fuco did not correlates heavily with Hex and But (Table 4), thus most of the Fuco must have originated from diatoms, not from coccolithophores or chrysophytes. Here, we validate that Fuco is a marker pigment for

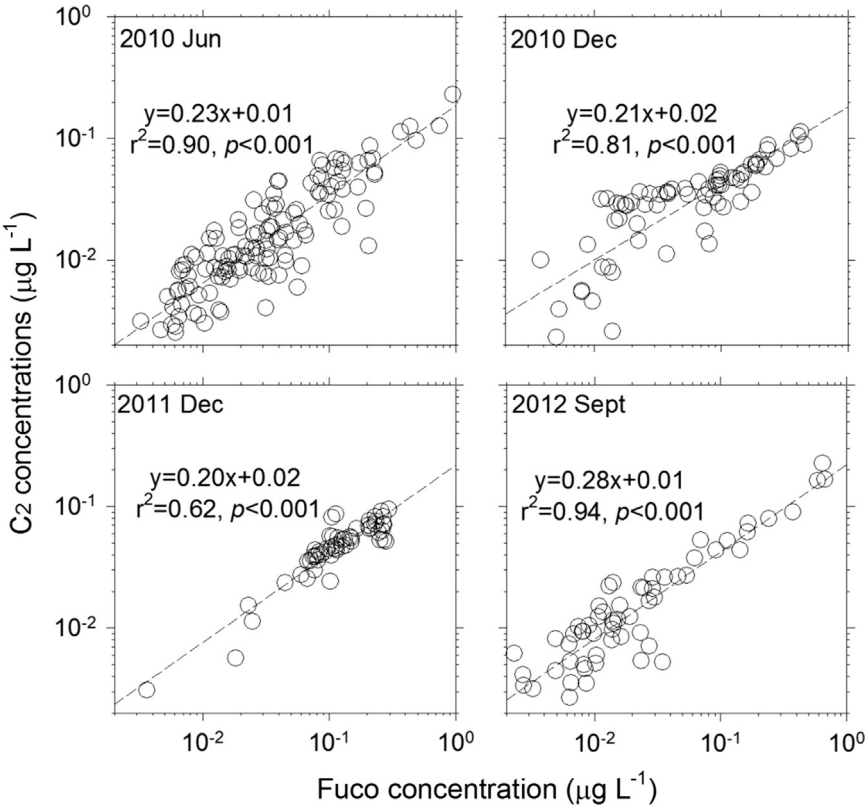

Fig. 14. The concentration correlation between Fuco and Chl *c2* among different seasons.

diatom in the NSCS, which is a major phytoplankton group in both the coastal and inner shelf regions of the NSCS during all seasons.

4.4. Chl b, Pras, Per, and Allo

Chl *b*, one of the most abundant pigments observed in oceanic coastal regions (Egeland et al., 1995), also exhibits elevated concentrations from the coastal region to the offshore water in the NSCS with maximum concentrations up to 0.30 μg L^{-1} or equivalently to 25–50% of Chl *a* concentrations in the offshore water (Figs. 2–5). It should be noted that the Chl *b* data shown in the figures include both mono-Chl *b* and divinyl chlorophyll *b* as we did not analytically separate DV Chl *b* from Chl *b*. Thus, Chl *b* shown in the figures may come from four different phytoplankton classes, *Pro*, prasiophytes, chlorophytes, and englenophytes. Quantitative estimates for their relative abundance is challenging without information of existing groups. The importance of chlorophytes as the sources of Chl *b* can be excluded first because the concentrations of its major pigment, Lut, were extremely low in entire studied sites, generally ranging from 0.001 to 0.005 μg L^{-1} or even below detection limit. Similarly, in terms of englenophytes, the concentrations of its marker pigment, diadino, were also extremely low in the studied site thus euglenophytes are also unlikely to be a major phytoplankton in the NSCS.

As discussed previously, *Pro* has been a major group in the offshore water of the NSCS, shown by the relatively high DV Chl *a* concentrations and *Pro* abundance observed. In addition to *Pro*, prasiophytes may also account for a large portion of the Chl *b* observed in the NSCS. The published marker pigment in prasiophytes, Pras, to Chl *a* ratio in prasiophytes is 0.024, about one fifth of its Chl *b* to Chl *a* ratio in prasiophytes, 0.131 (Egeland et al., 1995; Mackey et al., 1996; Lewitus et al., 2005). We found that the Pras to total Chl *b* ratio in our data was roughly 0.10. Using 0.20 as a Pras to Chl *b* ratio in prasiophytes, prasiophytes may account for 50% of the total Chl *b* measured in the coastal region. Our observation is consistent with a recent study using a molecular biology approach to evaluate the relative amount of different Pico groups, which reported that prasiophytes accounted for about 20% of Pico abundance in the NSCS in January 2010 (Wu et al., 2013). Overall, prasiophytes and *Pro* were two major phytoplankton groups contributing to the total Chl *b* measured. Since the DV Chl *a* and Chl *b* contours shown in the Figs. 2 and 3 are not comparable in the coastal region, prasiophytes should be the dominant group possessing Chl *b* in the coastal region. We also observe a strongly linear correlation between Chl *b* and But in the two summer cruises (Table 4). Since But and Hex are known to come from haptophytes in the NSCS, the strong linear correlation suggests that the two phytoplankton groups, prasiophytes and haptophytes, may have similar ecological niches during the summer season in the NSCS.

Three other coastal type pigments, peridinin, prasinoxanthin and alloxanthin, are specific markers for dinoflagellates, prasinophytes, and chryptophytes, respectively. They exhibited elevated value mainly in the coastal region of the NSCS, with maximum concentrations located within 100 km in the coastal waters (Figs. 2–5). The maximum concentrations of Per ranged from 0.01 to 0.03 μg L^{-1} and were only equivalent to 1–3% of the total Chl *a* in the coastal region at most (Mackey et al., 1996; Zapata et al., 2012). The maximum concentrations of Pras ranged from 0.01 to 0.02 μg L^{-1}. Different types of prasiophytes contain significantly different Pras to Chl *a* ratios so that the possible range of Pras to Chl *a* ratios would be relatively large. Applying 0.025 Pras to Chl *a* ratio (Mackey et al., 1996), the Pras concentrations, ranging from 0.01 to 0.02, were equivalent to 0.40–0.80 μg L^{-1} of Chl *a*, further supporting the notion that prasiophytes were a major phytoplankton group in the coastal water. During the summer cruises, Pras also extended into the offshore water, particularly during the September occasion (Figs. 2 and 5). Allo also exhibited a similar

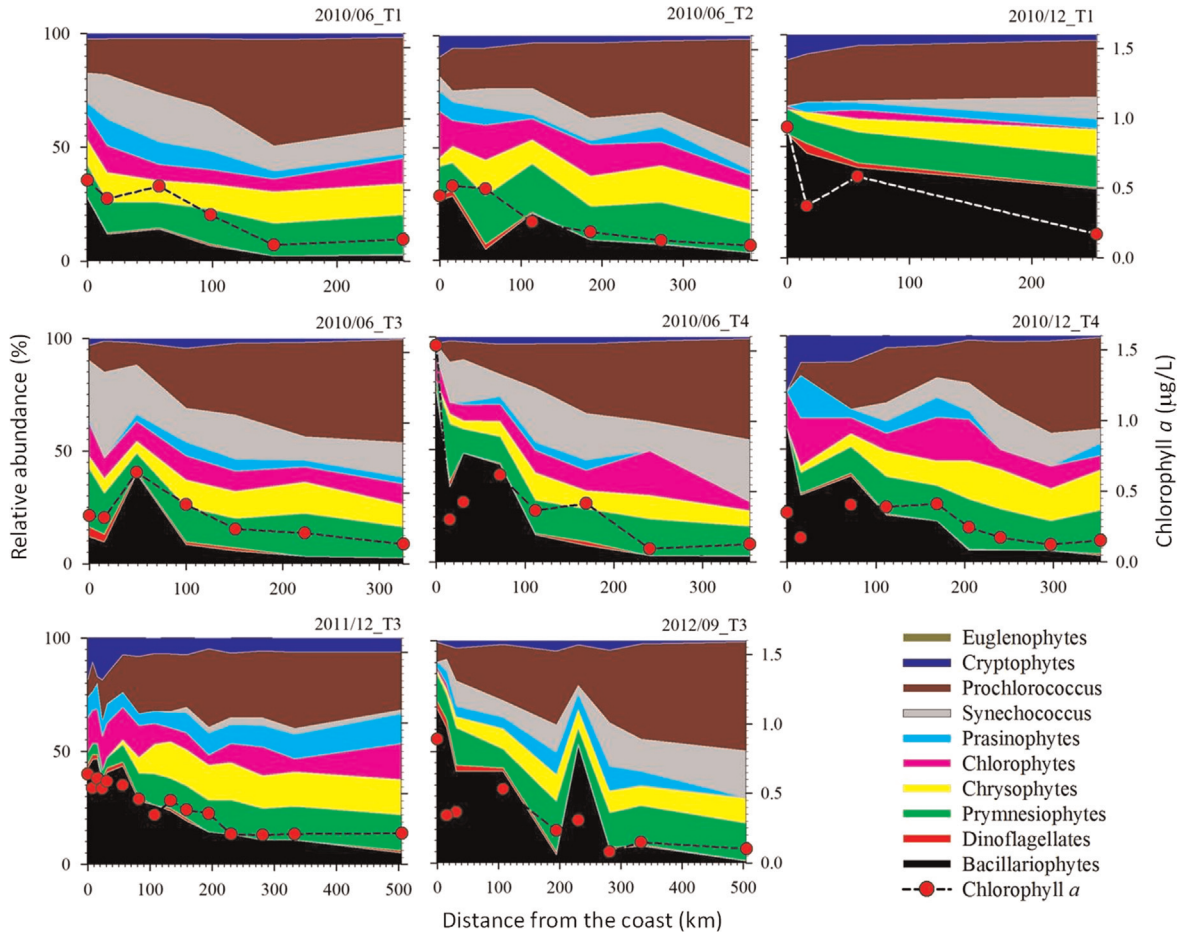

Fig. 15. Integrated total Chl *a* concentrations observed and the horizontal variations of relative abundance of phytoplankton groups estimated by CHEMTAX in the four transects during different cruise cruises. Total Chl *a* concentrations were used in the CHEMTAX calculation. Initial marker pigment to Chl *a* ratios used in the calculation are obtained from the averages of the maximum and minimum pigment value presented by Mackey et al. (1996). We ran the program by using cluster analysis and successive running to reduce the uncertainty (Latasa, 2007). Two winter pigment data are pooled together for successive final pigment ratio running. Similarly, two summer pigment data are also pooled together. The summer data are further separated to two layers, top 50 and below 50 m for successive running to obtain final pigment ratio output. The best 10% of the solutions with the lowest root mean square errors provided by CHEMTAX were averaged as the starting ratios. The final pigment ratios were then determined by CHEMTAX with the input of the starting ratios. The relative Chl *a* concentrations for each taxonomic group or their relative abundance (%) were calculated based on the final pigment ratios.

distribution pattern as Pras, with elevated concentrations observed in the coastal region with maximum concentrations ranging from 0.01 to 0.04 μg L^{-1}, accounting for 6 to 18% of total Chl *a* in the coastal region by using 0.3 pigment to Chl *a* ratio (Mackey et al., 1996; Lewitus et al., 2005). Overall, the abundance of dinoflagellates and chryptophytes was relatively low in the coastal region of the NSCS, and prasiophytes were found to be a major phytoplankton group in the coastal region of the NSCS.

4.5. CHEMTAX output and future challenge

By using the pigment data obtained in this study, we have run the CHEMTAX program to quantitatively estimate the relative contribution of the major phytoplankton groups in the NSCS. Some of the program output results are shown in Fig. 15. The running conditions are briefly described in Fig. 15. The distribution patterns of the relative abundance of the major phytoplankton groups are similar to the horizontal and vertical distribution patterns what we have observed by major pigment concentrations and ratios (Figs. 2–5). Overall, *Pro* and bacillariophytes (diatom) were the dominant phytoplankton groups in offshore and inshore regions, respectively. Their relative abundance may account for 30–50% in their dominant regions. The relative percentages of diatoms abundance decrease from the coast to the offshore region; the percentages of *Pro* abundance increase from the coast to the offshore region. *Syn* and prymnesiophytes (coccolithophores) were the other two major groups in the water. The relative abundance of both groups tends to decrease from offshore to inshore waters for most of the transects. However, the relative abundance of *Syn* was fairly consistent in both the inshore and offshore regions for the four transects in June 2010. Increasing relative abundance of cryptophytes was found in the coastal region during winter times, suggesting the intrusion of freshwater. In terms of prasinophytes and chrysophytes, compared to our previous derivation based on pigment concentrations, we believe that the relative abundance of prasinophytes may be underestimated and the relative abundance of chrysophytes may be overestimated by the CHEMTAX calculation. Although CHEMTAX program has been widely used to quantitatively estimate the relative abundance of marine phytoplankton groups during the past two decades (Mackey et al., 1996; Zepata et al., 2000; Latasa, 2007), it should be particularly noted that the accuracy of the CHEMTAX results need to be validated by other independent approaches, such as microscopic cell counting. The application of CHEMTAX in the NSCS is particularly challenging due to the complicated biogeochemical domains and features observed. In addition, relatively limited information is available for the major phytoplankton groups and their pigment ratios in the huge marginal sea. Conceptually, it should be ideal to run

CHEMTAX program by separating the NSCS data into individual biogeochemical domain for different seasons. By using different grouping approaches or marker pigment ratios, we found that we would obtain significantly different outputs from the results shown in Fig. 15, indicating that a large uncertainty in the calculation may exist. There are several possible reasons for the large uncertainty.

First, our studied sites cover estuarine, coastal, shelf, and deep water regions. The environmental conditions in the diverse domains, e.g., light intensity or nutrient status, result in varying pigment ratios for different specific phytoplankton groups and complicate the calculation, witnessed by the results shown in Figs. 11 and 12. The sampling points of this study should be insufficient when the data are separated into various domains in different seasons. Secondly, the information of major phytoplankton groups and their pigment ratios in the studied regions is not well known spatially and temporally. For example, the importance of euglenophytes or chlorophytes remains unclear among different transects as the group does not possess abundant unique specific marker pigments to confirm their existence. In winter season, different phytoplankton groups from the Taiwan Strait may be introduced into the coastal and shelf region of the NSC by the prevailing winter monsoon. Thus other phytoplankton groups also need to be considered, such as cryptophytes. In addition, the concentrations of some key pigments were not accurately resolved in this study. The analytical method of this study did not separate DV Chl *b* from mono-Chl *b*. Pras concentrations detected were generally low in pigment samples simply because the cellular pigment concentrations are relatively low in prasinophytes, which is known to be a major Pico group in the NSCS. Large volume sampling is required to obtain accurate Pras concentrations in the future studies. These analytical uncertainties in pigment samples would also considerably increase the uncertainty of the CHEMTAX calculation. Further effort should be applied to other independent methods (e.g., microscope) to identify the major phytoplankton groups in the diverse domains during different seasons, when hydrographic parameters can be simultaneously determined. Long term field observation with high temporal and spatial resolution is needed in the various domains of the huge marginal sea. The concentrations of DV Chl *b* and Pras need to be accurately measured. With the major phytoplankton group information, marker pigment to Chl *a* ratio data, and temporally and spatially sufficient pigment data in individual biogeochemical domains, we may better constrain the boundaries of each domain. Only then may CHEMTAX provide reliable and accurate quantitative estimate for phytoplankton community structure in the NSCS. For now, the CHEMTAX results shown should be considered to be preliminary and semi-quantitative.

About a decade ago, a comprehensive study investigating primary production reported that nitrogen was the major limiting factor for phytoplankton growth during spring and fall seasons in the NSCS (Chen, 2005). Our study indicates that P may have already become a limiting factor for phytoplankton growth in the NSCS during summer or late summer period, witnessed by depleted phosphate concentrations and their strong correlation with Chl *a* concentrations. This can be attributed to the increasing and lasting input of highly N enriched nutrient sources originating from terrestrial sources or anthropogenic activities. It would be interesting to investigate whether the nutrient status in the NSCS undergoes a seasonal cycle, from N-depleted mode in early summer to P-depleted status in late summer or autumn in high riverine discharge season and then to nutrient replete conditions during winter and spring time. The elemental and isotopic composition in some environmental recorders, such as coral cores, may be investigated to validate whether nutrient status may have changed during the past few decades in the NSCS. This information will also be useful in predicting the trend of future nutrient status change. Long term time series monitoring for the temporal and spatial variations of major nutrients and pigment concentrations is essential to elucidate the future interaction between changing nutrient status and the variations of phytoplankton community structure in the NSCS.

5. Conclusion

This study presents the temporal and spatial variations of pigment distribution in the NSCS and their environmental control. Coupling pigment distribution with cell abundance data, the vertical and seasonal variations of some cellular marker pigment concentrations are obtained for some major phytoplankton groups, which becomes useful information to establish algorithms between the marker pigments and their corresponding phytoplankton groups in the NSCS. Based on the relative distribution of some marker pigments, we have deduced the major phytoplankton groups both in the coastal and offshore water in different seasons. Spatially, the major phytoplankton groups in the coastal regions are diatom, prasinophytes, coccolithophores, and *Syn*; the major groups in the offshore water are *Pro*, coccolithophore, *Syn*, and diatom. Overall, the relative percentages of diatom abundance decrease from the coast to the deep water region; the relative percentages of coccolithophores abundance increase from the coast to the deep water region. The coupling effects of seasonal climate forcings and increasing terrestrial nutrient supply originating from anthropogenic activities regulate the temporal and spatial variations of the pigment distribution. With ongoing regional and global environmental changes, lasting dynamic shifts of the pigment composition and phytoplankton community structure in the Northern South China Sea are expected to be observed.

Acknowledgment

We thank the reviewers for providing valuable comments, which have greatly improved the quality of our manuscript. We thank Claudia Chern for proofreading this manuscript. We thank the crew members of OR/1 and OR/3 for helping seawater sampling. This work was financially supported by National Science Council Taiwan through Grants 101-2611-M-001-002 and 102-2611-M-001-004-MY3 and by Academia Sinica through the grant titled “Ocean Acidification: Comparative biogeochemistry in shallow water tropical coral reef ecosystems in a naturally acidic marine environment”.

References

Barlow, R.G., Cummings, D.G., Gibb, S.W., 1997. Improved resolution of mono- and diviynl chlorophylls *a* and *b* and zeaxanthin and lutein in phytoplankton extracts using reverse phase C-8 HPLC. Mar. Ecol. Prog. Ser. 161, 303–307.

Behrenfeld, M.J., Falkowski, P.G., 1997. Photosynthetic rates derived from satellite-based chlorophyll concentration. Limnol. Oceanogr. 42, 1–20.

Cai, Y.M., Ning, X.R., Liu, C.G., Hao, Q., 2007. Distribution pattern of photosynthetic picoplankton and heterotrophic bacteria in the Northern South China Sea. J. Integr. Plant Biol. 49, 282–298.

Cai, W.J., Dai, M.H., Wang, Y.C., Zhai, W.D., Huang, T., Chen, S.T., Zhang, F., Chen, Z.Z., Wang, Z.H., 2004. The biogeochemistry of inorganic carbon and nutrients in the Pearl River estuary and the adjacent Northern South China Sea. Cont. Shelf Res. 24, 1301–1319.

Chen, B.Z., Wang, L., Song, S.Q., Huang, B.Q., Sun, J., Liu, H.B., 2011. Comparisons of picophytoplankton abundance, size, and fluorescence between summer and winter in northern South China Sea. Cont. Shelf Res. 31, 1527–1540.

Chen, Y.L.L., 2005. Spatial and seasonal variations of nitrate-based new production and primary production in the South China Sea. Deep-Sea Res. I 52, 319–340.

Du, C., Liu, Z., Dai, M., Kao, S.J., Cao, Z., Zhang, Y., Huang, T., Wang, L., Li, Y., 2013. Impact of the Kuroshio intrusion on the nutrient inventory in the upper northern South China Sea: insights from an isopycnal mixing model. Biogeosciences 10, 6419–6432.

Egeland, E.S., Eikrem, W., Throndsen, J., Wilhelm, C., Zapata, M., Liaaen-Jensen, S., 1995. Carotenoids from further prasinophytes. Biochem. Syst. Ecol. 23, 747–755.

Furuya, K., Hayashi, M., Yabushita, Y., Ishikawa, A., 2003. Phytoplankton dynamics in the East China Sea in spring and summer as revealed by HPLC-derived pigment signatures. Deep-Sea Res. II 50, 367–387.

Goericke, R., Repeta, D.J., 1993. Chlorophylls *a* and *b* and divinyl chlorophylls *a* and *b* in the open subtropical North Atlantic Ocean. Mar. Ecol. Prog. Ser. 101, 307–313.

Ho, T.Y., Chou, W.C., Wei, C.L., Lin, F.J., Wong, G.T.F., Lin, H.L., 2010. Trace metal cycling in the surface water of the South China Sea: vertical fluxes, composition, and sources. Limnol. Oceanogr. 55, 1807–1820.

Huang, B.Q., Hu, J., Xu, H.Z., Cao, Z.R., Wang, D.X., 2010. Phytoplankton community at warm eddies in the northern South China Sea in Winter 2003/2004. Deep-sea Res. Part II 57, 1792–1798.

Huang B.Q., 2013. Phosphorus stress of phytoplankton in the eastern and northern South China Seas. In: AOGS Meeting. Session BG08-OS19-A009.

Jan, S., Wang, J., Chern, C.S., Chao, S.Y., 2002. Seasonal variation of the circulation in the Taiwan Strait. J. Mar. Syst. 35, 249–268.

Latasa, M., 2007. Improving estimations of phytoplankton class abundances using CHEMTAX. Mar. Ecol. Prog. Ser. 329, 13–21.

Lewitus, A.J., White, D.L., Tymoswki, R.G., Geesey, M.E., Hymel, S.N., Noble, P.A., 2005. Adapting the CHEMTAX method for assessing phytoplankton taxonomic composition in the southeastern U.S. estuaries. Estuaries 28, 160–172.

Lien, R.C., Tang, T.Y., Chang, M.H., D'Asaro, E.A., 2005. Energy of nonlinear internal waves in the South China Sea. Geophys. Res. Lett. 32, L05615. http://dx.doi.org/10.1029/2004GL022012.

Liu, H.C., Shih, C.Y., Gong, G.C., Ho, T.Y., Shiah, F.K., Hsieh, C.H., Chang, J., 2013. Discrimination between the influences of river discharge and coastal upwelling on summer microphytoplankton phosphorus stress in the East China Sea. Cont. Shelf Res. 60, 104–112.

Liu, Q., Dai, M., Chen, W., Huh, C.A., Wang, G., Li, Q., Charette, M.A., 2012. How significant is submarine groundwater discharge and its associated dissolved inorganic carbon in a river-dominated shelf system? Biogeosciences 9, 1777–1795.

Mackey, M.D., Mackey, D.J., Higgins, H.W., Wright, S.W., 1996. CHEMTAX-a program for estimating class abundance from chemical markers: application to HPLC measurements of phytoplankton. Mar. Ecol. Prog. Ser. 144, 265–283.

Moore, L.R., Goericke, R., Chisholm, S.W., 1995. Comparative physiology of *Synechococcus* and *Prochlorococcus*: influence of light and temperature on growth, pigments, fluorescence and absorptive properties. Mar. Ecol. Prog. Ser. 116, 259–275.

Ning, X.R., Li, W.K.W., Cai, Y.M., Shi, J.X., 2005. Comparative analysis of bacterioplankton and phytoplankton in three ecological provinces of the northern South China Sea. Mar. Ecol. Prog. Ser. 293, 17–28.

Pan, X.J., Wong, G.T.F., Ho, T.Y., Shiah, F.K., Liu, H.B., 2013. Remote sensing of picophytoplankton distribution in the Northern South China Sea. Remote Sens. Environ. 128, 162–175.

Pan, X.J., Wong, G.T.F., Tai, J.H., Ho, T.Y., 2015. Climatology of physical and biological characteristics of the Northern South China Sea Shelf-sea (NoSoCS) and adjacent waters: observations from satellite remote sensing. Deep-Sea Res. II 117, 10–22. http://dx.doi.org/10.1016/j.dsr2.2015.02.022.

Tseng, C.M., Wong, G.T.F., Lin, I.I., Wu, C.R., Liu, K.K., 2005. A unique seasonal pattern in phytoplankton biomass in low-latitude waters in the South China Sea. Geophys. Res. Lett. 32, L08608. http://dx.doi.org/10.1029/2004GL022111.

Wong, G.T.F., Pan, X., Li, K.Y., Shiah, F.K., Ho, T.Y., Guo, X., 2015. Hydrography and nutrient dynamics in the Northern South China Sea Shelf-sea (NoSoCS). Deep-Sea Res. II 117, 23–40. http://dx.doi.org/10.1016/j.dsr2.2015.02.023.

Wu, C.R., Hsin, Y.C., 2012. The forcing mechanism leading to the Kuroshio intrusion into the South China Sea. J. Geophys. Res. 117, C07015. http://dx.doi.org/10.1029/2012JC007968.

Wu, W., Huang, B., Zhong, C., 2014. Photosynthetic picoeukaryote assemblages in the South China Sea from the Pearl River estuary to the SEATS station. Aquat. Microb. Ecol. 71, 271–284.

Xu, J., Yin, K.D., He, L., Yuan, X.C., Ho, A.Y.T., Harrison, P.J., 2008. Phosphorus limitation in the northern south china sea during late summer: influence of the pearl river. Deep-Sea Res. I 55, 1330–1342.

Yin, K.D., Song, X.X., Sun, J., Wu, M.C.S., 2004. Potential P limitation leads to excess N in the Pearl River estuarine coastal plume. Cont. Shelf Res. 24, 1895–1907.

Zepata, M., Rodríguez, F., Garrido, J.L., 2000. Separation of chlorophylls and carotenoids from marine phytoplankton: a new HPLC method using a reversed phase C8 column and pyridine-containing mobile phases. Mar. Ecol. Prog. Ser. 195, 29–45.

Zapata, M., Jeffrey, S.W., Wright, S.W., Rodriguez, F., Garrido, J.L., Clementson, L., 2004. Photosynthetic pigments in 37 species (65 strains) of Haptophyta: implications for oceanography and chemotaxonomy. Mar. Ecol. Prog. Ser. 270, 83–102.

Zapata, M., Rodríguez, F., Fraga, S., Barra, L., Ruggiero, M.V., 2011. Chlorophyll c pigment patterns in 18 species (51 strains) of the genus *Pseudo-nitzschia* (Bacillariophyceae). J. Phycol. 47, 1274–1280.

Zapata, M., Fraga, S., Rodríguez, F., Garrido, J.L., 2012. Pigment-based chloroplast types in dinoflagellates. Mar. Ecol. Prog. Ser. 465, 33–52.

Zhai, H.C., Ning, X.R., Tang, X.X., Hao, Q., Le, F.F., Qiao, J., 2011. Phytoplankton pigment pattern and community composition in the northern South China Sea during winter. Chin. J. Oceanol. Limnol. 29, 233–245.